NASA CONTRACTOR REPORT

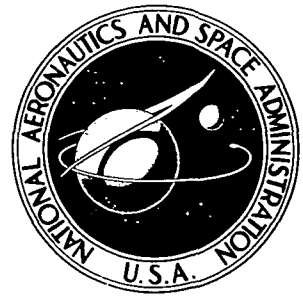

NASA CR-2469

NASA CR-2469

EFFECT OF INTERJET SPACING ON MIXING OF MULTIPLE COAXIAL JETS IN SUPERSONIC FLOW

by A. K. Lorber and J. A. Schetz

Prepared by
VIRGINIA POLYTECHNIC INSTITUTE AND STATE UNIVERSITY
Blacksburg, Va. 24061
for Langley Research Center

NATIONAL AERONAUTICS AND SPACE ADMINISTRATION • WASHINGTON, D. C. • DECEMBER 1974

1. Report No.	2. Government Accession No.	3. Recipient's Catalog No.
NASA CR-2469		

4. Title and Subtitle	5. Report Date
EFFECT OF INTERJET SPACING ON MIXING OF MULTIPLE COAXIAL JETS IN SUPERSONIC FLOW	December 1974
	6. Performing Organization Code

7. Author(s)	8. Performing Organization Report No.
A. K. Lorber and J. A. Schetz	VPI-Aero-015
	10. Work Unit No.

9. Performing Organization Name and Address	11. Contract or Grant No.
Virginia Polytechnic Institute and State University Blacksburg, Virginia 24061	NAS1-10233
	13. Type of Report and Period Covered
12. Sponsoring Agency Name and Address	Contractor Report
National Aeronautics and Space Administration Washington, D.C. 20546	14. Sponsoring Agency Code

15. Supplementary Notes

Final Report

16. Abstract

An experimental and analytical investigation of strut-mounted, four-nozzle, downstream facing, gaseous fuel injector assembly was conducted in a Mach 4 airstream with P = 154 psia and T_o = 520°R. Helium was used as the injectant, and the interjet spacing (S/D) was the main parameter varied. The principal data are in the form of Helium concentration profiles at seven axial stations, Mach number distributions at three axial stations and Schlieren photographs of the flow field at different interjet spacings. An approximate analysis was developed based upon a linearization in the Von Mises plane, Crocco integrals for the temperature and concentrations fields and an eddy viscosity model. Good agreement with the data was achieved. It was found that, at these conditions, interjet spacing has an effect on mixing only up to S/D of approximately 2.5, with concentration of injectant becoming smaller as S/D is increased, and the Mach number downstream of the injector tends to decrease with decreasing S/D.

17. Key Words (Suggested by Author(s))	18. Distribution Statement
Jet Mixing Fuel Injection Supersonic Combustion	Unclassified - Unlimited STAR Category: 12

19. Security Classif. (of this report)	20. Security Classif. (of this page)	21. No. of Pages	22. Price*
Unclassified	Unclassified	88	$4.75

*For sale by the National Technical Information Service, Springfield, Virginia 22151

TABLE OF CONTENTS

Page intentionally left blank

LIST OF FIGURES

LIST OF TABLES

Page intentionally left blank

NOMENCLATURE

a	jet radius = D/2
D	jet diameter
$K_{2\pi}$	a constant equal to 0.018
M	Mach number
P_c	cone static pressure
P_t	Pitot pressure
r	radial distance from nozzle centerline
S	centerline to centerline spacing
S/D	non-dimensional interjet spacing
X	axial coordinate
X/D	non-dimensional downstream distance
u	velocity
U	u/u_e
ε	eddy viscosity
ρ	density
ψ	transformed radial distance
ξ	transformed axial distance

Subscripts

c	jet centerline
e	free stream
j	jet
δ	at the outer edge of the mixing zone

EFFECT OF INTERJET SPACING ON MIXING OF MULTIPLE COAXIAL JETS IN SUPERSONIC FLOW

A. K. Lorber and J. A. Schetz

Virginia Polytechnic Institute and State University

Blacksburg, Virginia 24061

I. INTRODUCTION

Air breathing engines have now advanced to the point where conventional ramjet engines in which the combustion process takes place in a subsonic internal flow are a practical reality. As hypersonic flight has begun to be contemplated, it has been shown (Ref. 1, 2) that, in this flight regime, a ramjet engine with a supersonic flow through the combustor (a SCRAMjet) will be superior to one with subsonic combustor flow, provided that the required combustor length is not excessive. A minimum length combustor is required in order to minimize the cooling load in this high heat transfer rate region. While current rocket motors can easily accelerate vehicles to hypersonic speeds, air breathing engines are considerably more efficient, due to their much higher specific impulse. (Ref. 3).

In order to achieve an acceptable combustion efficiency in a short length, it is necessary to provide for rapid mixing, ignition and combustion. With a supersonic combustor flow, the type of flame stabilizers and mixing aids used in subsonic engines (Ref. 4) are unacceptable. The mixing of the fuel can be achieved by injecting perpendicular to the air flow (Ref. 5, 6, 7), from rearward facing steps (Ref. 8) or from rearward facing nozzles (Ref. 9). Obviously, the details of the mixing process will also depend upon whether a liquid or gaseous fuel is to be employed. With high energy fuel such as Hydrogen, which is generally accepted as a fuel for such an engine due to its superior performance characteristics (Ref. 6) it will not be practical to construct an upstream facing nozzle, although undoubtedly this would enhance mixing.

While perpendicular injectors are efficient from a mixing and ignition point of view (Ref. 10), they produce shock waves which lower the total pressure in the combustor and thus degrade performance. Wall mounted rearward facing slots generally fail to provide sufficient penetration of the fuel into the center of the combustor. A rearward facing nozzle (or array of nozzles) located out in the combustor flow (jet injector) might provide for a suitable distribution of fuel across the airstream. However, such nozzles require supports which produce shocks and, therefore, losses. Practical engines may well employ a combination of wall and jet injectors. An important consideration, then, will be the interference (constructive or destructive) on adjacent, co-axial, turbulent mixing flows. Our attention here will be focused upon gaseous injection from relatively closely spaced downstream facing jets in a supersonic airstream.

The general problem of the diffusion of a foreign gas from a downstream facing nozzle into a co-flowing stream is not a new one. Essentially this is the familiar problem of turbulent mixing of co-axial jets which has been the subject of considerable study throughout this century. Ref. 11 presents a comprehensive summary of work prior to 1960. Due to the complexity of turbulent flows in general, all "theoretical" work draws heavily upon experimental work. Ref. 12 contains a tabulation of experimental work published up to 1969. Ref. 13 presents a critical review of existing theories, compares them with experimental results and tries to predict which ones will have application for a wide range of problems. The recent NASA workshop on free turbulent shear flows (Ref. 14) provides a ready assessment of the state of the art as of last year.

While the large body of information described in the references cited above is of considerable interest here, the design of a successful SCRAMjet is still limited by inadequate fuel diffusion from isolated injectors. A solution which appears to be attractive is the mounting of downstream facing jets in clusters. The improvement in fuel dispersion is achieved by the fact that for a given rate of flow of fuel, the volume of the mixing region per unit length downstream from the nozzle, increases with the number of nozzles.

The two important quantities to be investigated in such a configuration will be the spacing between the individual nozzles and its effect on the mixing characteristics, and the interaction between the different jets after they start merging. The non-dimensional spacing, S/D, is used to parameterize the problem. The only applicable previous study is Ref. 15 which describes a preliminary work in which two values of S/D (4.0 and 2.8) were investigated at a free stream Mach number of 4.0. The configuration consisted of five nozzles located on a crossed strut that was swept to the flow. Little effect of S/D on mixing rates was noted. Apparently the S/D's chosen were too large and the results were inconclusive. Also, this arrangement produced a rather large disturbance in the mixing region. A further problem was encountered in achieving an equal distribution of the total injectant through each of the individual nozzles.

Based upon the results of this first study a further effort was planned to employ a better designed model which would provide a lesser disturbance and enable study of smaller S/D's. The present report describes the results of an experimental and theoretical study of a variable S/D injection system in a Mach 4 airstream utilizing Helium as the injectant to simulate Hydrogen without safety problems. The major parameter varied was the centerline to centerline jet spacing, (S/D of 1.5 - 3.0) and the principal data consist of Helium concentration distributions, obtained by chemical analysis. Mach number surveys downstream of the injectors and schlieren pictures were also made. In the first section of this report, a complete description of the equipment, instrumentation, and test methods employed is given. Then, the experimental results are presented and discussed. Finally, a theoretical method for the calculation of such problems is presented and compared to the experimental results.

II. APPARATUS AND TEST PROCEDURE

A. Wind Tunnel Facilities

Tests were conducted in the 9" x 9" supersonic wind tunnel in the Gas Dynamics Lab at V.P.I. & S.U. This facility is of an intermittent, blow-down type with interchangeable contoured nozzles. The Mach 4.016 nozzle was used for this experimental effort. The nominal starting tunnel total pressure and temperature were 154 psia and 530°R, respectively. During the tests there was a slow linear decrease in both total pressure and total temperature. In order to account for these variations all recorded pressures were nondimensionalized by their corresponding stagnation conditions at the time the measurements were taken. Test runs were approximately 8 seconds in duration. A full description of the supersonic wind tunnel used in these tests is presented in Appendix B.

B. Description of the Model

For the present series of tests, an injection system model was designed to meet the following criteria. First, variable interjet spacing, S/D, was required. Indeed, the primary purpose of the tests was to establish the influence of S/D on mixing characteristics. Instead of building several models with different spacings between the nozzles it was felt it would be advantageous to build a single model in which the distance between the injectors could be changed over a wide range by simple adjustment. While this was considerably more complicated mechanically, it was felt that the flexibility and the use of the same set of nozzles for all configurations to yield more consistent data would justify this effort. Second, it was desired that the model would cause a minimum blockage of the wind tunnel and the minimum possible disturbance to the flow. Next, it was important to have individual lines feeding the injectant to each of the nozzles. This alleviated, as will be shown later, most of the problems of achieving matched flow fields at the exits of the individual nozzles. It was also believed that a model in which all injectors would be identical, both at their leading and trailing edges, and would exit into identical flow fields will give a better understanding of the flow, particularly with a view to

configuration with more than four or five nozzles. Finally it was deemed important to make the present model as accurate as possible, in order to minimize variations in the flow field due to inaccuracies in the model, especially for the low S/D ratios to be considered. This required a design that could be produced by machine tools with the least amount of hand work.

The injector model which resulted is presented in Fig. 1a, c, and d; photographs of it are presented in Fig. 1b. It consisted of four separate injectors arranged in pairs; one pair extending from the tunnel "floor" and the other from the "ceiling." Each injector consisted of a stainless steel support strut, which also served as the injectant feed line, and a nozzle. The strut cross section was two inches long. Its thickness was 0.44" for the outer section and 0.31" for the inner section. Leading and trailing edges were wedges with half angles of 23.75° and 17.25°, for outer and inner sections respectively. For the first 3.0 inches of their length the struts in each pair are parallel and at a distance of approximately 3.25 inches from each other. Then, the two struts are bent towards the center at an angle of 45°. The ends of the struts, terminated by the injector nozzles, are at a distance of approximately 0.6 inches from each other. The actual distances between the struts and between the nozzles can be varied as will be explained shortly.

The injector nozzles consisted of stainless steel tubes (0.25" O.D. and 0.190" I.D.) brazed to the struts parallel to the tunnel axis. The leading edges of the nozzles are 7° half angle cones made of brass and brazed to the nozzles in such a way that the side of the cone towards the center of the model (looking from the rear, the one at 45° from the horizontal) was parallel to the flow. This was done in order to achieve as undisturbed a flow as possible in the region between the nozzles. The 7° half angle was chosen as the thinnest cone feasible without being too delicate to handle. The struts were drilled through to provide passage for the injectant into the nozzles.

In order to achieve variable S/D the bases of the struts were machined in a series of 0.0625" steps parallel to the flow, and fitted into a frame into which matching steps were machined. This frame was mounted directly into the nozzle of the wind tunnel. By realigning a given step on the strut with different steps in the frame, the strut was caused to change position, both vertically and horizontally, in increments of 0.0625". Thus, the distance between the struts in each pair changed by 0.125", and by the same amount from the second pair, in successive steps. The struts were then bolted to the supporting frame and to each other. The distance of 0.125" equalled 0.5 D and the actual values of S/D used were 1.5, 2.0, 2.5 and 3.0.

The reason for the 45° bend in the struts was that this provided a configuration which was symmetric about the tunnel axis in the area of interest and which remained so with varying S/D's.

C. Injectant Supply System and Test Conditions

The arrangement of the supply system is shown schematically in Fig. 2. The basic elements of the system are: 1) a nine bottle manifold for storage, 2) an electrically operated ball valve, 3) a dome regulator (Grove Powreactor Dome Controller Model RBX204-015) in parallel with a globe valve, 4) a mass flow measuring station and 5) copper tubing connectors to the top and bottom of the tunnel leading into the struts. (The globe valve was originally installed to act as a back-up system in case the dome regulator could not pass the required amount of injectant. It turned out, however, that the dome regulator could pass all the mass flow and the globe valve was kept closed).

Flow from the nine bottle manifold was initiated by the ball valve. Flow control was achieved by the dome regulator which was preset before a run. The flow rate was determined with an ASME Orifice Flow Meter (Ref. 16). The orifice was .600" diameter inside a 1.280" I.D. pipe. The flow rate was calculated using a standard procedure (Ref. 16) with pressures p_1 and p_2.

The total injectant flow rate was 1.83 lbs/min of pure Helium. This flow rate was kept within $^{+1.6}_{-1.3}$% of the prescribed flow for all tests with all

configurations. This was established on the spot by recorded readings of p_1 and p_2 and any run which diverged from these limits was repeated. The value of 1.83 lbs/min was chosen upon inspection of Schlieren photos of the flow. At this flow rate, the edge of the Helium flow emerging from the nozzles became discernible with no strong shocks apparent in the injectant stream.

The other injectant flow conditions, calculated using Ref. 17, were as follows:

Average Total Pressure (at exit): 27.1 psia
Total Temperature: 430°R
Static Temperature: 345°R
Velocity: 4250 ft/sec
Mach Number: at the exit 0.86*
after expansion 2.5
Reynolds number based on nozzle internal diameter: 48750

Free stream flow conditions in the wind tunnel, based on an average Mach number of 2.99 were as follows:

Total Pressure: 58.6 psia
Total Temperature: 520°R
Static Pressure: 1.6 psia
Static Temperature: 186°R
Density: 0.023 lbs cu/ft
Velocity: 2001 ft/sec
Renolds number based on strut chord (2.0 inch): 783000

D. Pressure and Gas Analysis Instrumentation

Pitot pressure and Helium concentration distributions were obtained to define the flow field. The Pitot pressure surveys were used with isolated cone-static measurements to obtain Mach number profiles of the flow.

---

*This is a one-dimensional average value.

With the rake shown in Fig. 3, Pitot pressure and gas sampling surveys were taken at several axial stations as follows: Gas samples at X/D of 1, 3, 6, 12, 24, 36 and 48 based on outside diameter of the nozzle which was 0.250", pressure readings at X/D of 0.1, 24 and 48. All sampling and pressure measurements were made at all four S/D's. The individual probes on the rake were constructed of 0.030" O.D. and 0.016" I.D. stainless steel tubing and they extended 0.25" from their mounting bars.

The large number of probes on the rake was required in order to cover all the areas of interest across the flow at any axial station without moving the rake. During the gas sampling runs this enabled taking 14 samples simultaneously along three axes: vertical, horizontal and diagonal. This enhanced the consistency of results while still giving fine enough coverage of the three-dimensional mixing zone for meaningful data. It should be pointed out, however, that certain probes on the rake (notably 4 and 5) gave inconsistent results. Tests for leaks proved negative but further tests on different nozzles, while being inconclusive, gave rise to the possibility that individual probes may exert an influence on each other, at least under the present flow conditions, and this possibility should be investigated in the future. Due to these uncertainties, Helium concentration data from probes 4 and 5 was not included in the presented results.

No satisfactory location could be found on the rake for a static pressure probe and so a separate one was constructed, see Fig. 3c. This was a 10° half angle brass cone. The base of the cone was 0.062" and the tip was precision ground to a sharp point. At 0.11" from the tip of the cone there were four 0.013" ports drilled perpendicular to the surface and 90° apart. The recorded pressure was the average of these four ports.

Two key devices were used in positioning the rake and the static probe for taking the surveys. A steel strut with a 14° wedge leading edge was used to hold the rake. The strut was 20.5" high with a base 6" by 1". There was a 0.625" diameter hole 20" above the base for the rake, and the base of the strut was bolted to a milling machine bed. This device was used for

both lateral and vertical positioning of the rake. The micrometer associated with the vertical location of the rake was graduated in 0.001". The micrometer which indicated lateral position was marked also in 0.001".

After the preliminary runs it was found that at the forward positions (low X/D) the rake support was not rigid enough. An additional support in the form of an adjustable triangular frame was added, which, when bolted to the tunnel floor, gave the required support, both to the rake and the static probe.

In all gas sampling runs, the rake was positioned so that probe No. 3 was centered in line with the geometric center of nozzle 3 (lower right, looking upstream). Positioning of the rake for the pressure runs is given schematically in Fig. 4. The static probe was located exactly as probe No. 3.

For the pressure runs, the leads from the rake were connected to a Model 48J9-1021 Scani-valve. Due to some large variations of pressure from port to port a scan rate of 0.5 seconds per port had to be accepted. Since the total useful run time was of the order of 8 seconds, two runs had to be performed for each station and certain amount of overlap was permitted to insure the correct numbering. A single transducer, a Statham PM 131 TC ± 50-350 SER 51926 ± PSID, was used in these tests. All pressures were read on a Hewlett-Packard strip chart recorders with a maximum deflection of 10", an accuracy of 0.1% of full scale setting and a response time of 0.25 sec.

When gas sampling tests were being run, the leads from the rake were run to a 14 bottle, solenoid valved collection cart shown in Fig. 5. The sampling lines and bottles were continuously purged by a vacuum pump, and during the actual sampling the flow was diverted into the individual bottles for 3 seconds. After the run the lines were again very thoroughly purged and the bottles were filled with Argon up to a pressure of 50 PSIG. The reason for this last operation lies in the fact that after the run the bottles were still at subatmospheric pressure, and the chemical analysis, which came next, required about 5 psig per run. The complete cart and each

sample bottle were leak checked by pressurization with pure Helium for 48 hours and at subatmospheric pressure for 72 hours. Spot checks were run every few days.

Analysis of the gas samples was done with a Perkin-Elmer Model 900 Gas Chromatograph with a Carle, 0.1 ml Sample loop, insertion valve. Results were obtained graphically on a Beckman 10" recorder Model 1005 and digitally by means of an "Autolab 6300" digital integrator. Each sample was run through the Gas Chromatograph at least twice and unless results were within 2 percent of each other (namely ±1.0%) the same sample was rerun until at least two runs came within this range. In most cases there was no need for the third run. Occasionally, notably with high Helium concentration samples, a third run was required and rarely a fourth. Detailed calibration and data reduction procedures are described in Appendix C.

E. Experimental Procedure

A typical run consisted of several operations in sequence and parallel, several of which had to be timed. After a few preliminary runs it became obvious that the operational load was too large for one person and an automatic timer (Cramer Controls, Model 540-4S, 8 poles) was introduced. All operations concerned with the run were tied to this timer. The sequence of operations and their timing is given in Table 1.

The total time of eight seconds was dictated by the length of the run of the tunnel, and, at that time, the timer came to an automatic stop so that a new cycle would not start again. The delay of three seconds before sampling was set to let the flow stabilize. This interval of 3 seconds was found (experimentally) to be more than twice of what was actually required to obtain a correct sample.

The pre-test set-up involved the following procedure. First, the Helium supply system was brought up to a pressure of approximately 550 psia and the flow rate was checked and adjusted. Next, the entire sample collection cart was pumped out to a vacuum of 400 millitorrs (0.4 mm of Hg) and

the vacuum pump was left running. The Schlieren system was checked and the tunnel air storage system was brought up to pressure. Just before the run, the sample bottles on the cart were closed (electrically) and the lines to the rake opened. The timer was then started and during the run the sampling bottles, which were under vacuum, opened, drew in the different samples and closed again.

After the run the whole cart except for the bottles was pumped out again and flooded with Argon at 70 psig. These last two steps were repeated three times and then, with the Argon pressure on, each bottle in turn was opened by hand and Argon was let in up to a pressure of 50 psig. This last step was done in this manner to insure that no sample escaped back into the cart's internal tubing system. After all the bottles were pressurized the cart was disconnected from the Argon supply and taken to analysis.

F. Optical Methods

Schlieren photographs were taken in order to optically visualize the flow field. A 12" Schlieren Apparatus with two parabolic mirrors, each having a focal length of 80" and an air cooled high intensity mercury-arc PEK light source was used with a 1 millisecond exposure. Photographs were taken on a polaroid type 56 (ASA 3000) sheet film using a Graphlex camera. All gas sampling runs and most of the pressure mapping runs were photographed in order to provide additional information about the flow field and in order to signal a malfunction or irregularity which might not have been registered by other means.

III. PRESENTATION OF DATA

A. Nozzle Flow Fields

Figure 6 depicts the total pressure distribution due to Helium injection from the nozzles at the nominal flow rate without the tunnel air flow. As can be seen, the profiles are almost identical, verifying the adequacy of the model and feed system. In an earlier test, discrepancies on the order of 50% were found at some points, but these were traced to dissimilar bends in the copper lines leading from the Helium manifold to the struts. After adjusting the bends in the lines by hand to make them as similar as possible, the present results were obtained. Nozzle 3 was chosen for all sampling runs and for those pressure runs centered on a nozzle. This choice, however, was purely a matter of convenience of working in the tunnel.

B. Schlieren Pictures

Schlieren photographs of the flow field with Helium injection are presented in Fig. 7. There are four such pictures depicting the flow with the nozzles at the different S/D's. The flow is from the left to the right and in three of the pictures the rake is visible. At S/D 2.0 and 2.5 the rake is at the X/D = 3 position and at S/D = 3.0 the rake is at X/D = 1.

In each of these pictures the general flow field is clearly visible as are the disturbances produced both by the structure of the strut and the jets emerging from the nozzles. The curved shock waves on the trailing edges of the struts in the upper and lower parts of the pictures are located at the bends of the struts which are not visible in these pictures.

An interesting feature of these pictures is the flow field between the nozzles. Due to the close proximity of the nozzles for small S/D the flow is disturbed, and this condition is relieved as the nozzles are separated from each other. The shock waves visible between the nozzles are probably located either between adjacent nozzles or in the center of the four nozzles. This conclusion is based on the following reasoning. The distance between the nozzles and the tunnel wall is more than four inches and each increment in S/D changes this distance by 0.0625". The distance between the nozzles

varies between 0.375" (S/D = 1.5) and 0.75" (S/D = 3.0) and each increment changes this distance by 0.125. The shocks themselves move each time about 0.180" forward or rearward. Evaluation of these numbers shows that the shocks must be located between the nozzles.

The Schlieren pictures also gave the first indication that the jet issuing from the nozzles may be underexpanded. This point was later verified when pressure measurements of the flow fields were taken and interpreted. The one-dimensional average Mach number of the jet just at the exit was found to be 0.86 and the Mach number of the jet immediately downstream of the nozzle was calculated to be 2.50.

Overall, the photos support the contention that this multiple-port injector system produces a nearly minimal disturbance in the Mach 4.0 free stream. Thus, the design should prove useful for practical applications.

C. Helium Concentration Profiles

The principal data obtained in this study are Helium concentration profiles for S/D 1.5, 2.0, 2.5 and 3.0. Each such configuration was tested at seven axial stations, namely X/D of 1, 3, 6, 12, 24, 36 and 48. The data was collected simultaneously along three axes; looking upstream, these were vertical, horizontal and diagonal (see also Fig. 3a for location of probes on each axis). All gas analysis data obtained are tabulated in Tables 2 to 5. Graphs, representative of the results, are presented in Figs. 8 to 19 inclusive.

Figures 8 to 10 give Helium concentration profiles across the nozzle in all three planes, i.e., vertical, horizontal and diagonal. As can be seen most of the data behave in the expected manner, that is, the concentration is highest at the center of the nozzle and falls off towards the edges, the maximum concentration falls off with axial distance and the concentration is lower for larger S/D. The only exception occurs (for both S/D's in the graphs, and, as can be seen from the tabulated results, in the other S/D's also) when going from X/D = 1 to X/D = 3. Here, the concentration increases in apparent defiance of elementary intuition. Since this behavior repeats

itself consistently for all S/D's, and similar results were obtained after some tests were repeated and double checked, the conclusion is that these results are valid. The most probable explanation lies in the realization that the injection system tested is a real one, meaning that the nozzles are supported by struts of relatively large size and there are strong interactions between the different nozzles and struts. The flow field, and this can also be ascertained by the Schlieren photographs, is disturbed by many weak shocks and reflections and this is probably what is causing this "inversion."

In order to further test this hypothesis another test was run at X/D = 0.1 with S/D = 3. The results are tabulated in Table 6 and given in Fig. 11. In this test another rake with different probe spacing was used. As can be seen, at this distance the concentration is at its expected high initial value since here the jet has not yet been influenced by most of the shock waves created by the flow downstream of the nozzle. Even at this point, however, the concentration did not come to 100% Helium, so another test was run using a special probe inserted about four nozzle diameters up into the nozzle itself. The reading obtained was 96%. Since the Helium used in these tests is practically pure (0.9995), this amount of contamination can be attributed to the cumulative effect of several factors: A helium tank had to be changed for each production run, and it is possible that minute quantities of air remained in the valves. Also, while particular effort was made to purge the cart each time by alternate pressurizing with argon and evacuation by the vacuum pump, again, minute quantities of air might have been trapped in the valves. Another possibility is the behavior of the gas chromatograph at very low concentrations of one of the constituents, and this is explained more in Appendix C. In view of these observations, the concentrations reported should probably be viewed as uncertain by about 3 - 4%. (See also Appendix A).

In order to better visualize the trends of the results, cross correlations of the concentrations were prepared and they are presented in Figs. 12 to 19. Fig. 12 is the plot of the maximum concentrations (disregarding their actual locations) as a function of axial distance for different S/D's.

Inspection of Fig. 12 shows again the unusual behavior of the concentration near the origin. Another interesting point is the effect of S/D on the concentration. As seen in this graph, S/D has a somewhat inconsistent effect on the concentration at lower X/D's, but starting at X/D = 36 the influence of S/D is clear and as expected, namely lower concentration at higher S/D. It also shows that the concentration is a function of S/D only up to S/D = 2.5, which corresponds to S = 0.625". This will explain the somewhat inconclusive results obtained in the work described in Ref. 15 in which the lowest S/D was 2.8.

Figures 13 - 19 give the concentrations obtained by certain probes, which in effect means the concentrations at certain points in the flow. (For brevity, location of points in the flow is denoted by probe number in that location.) An important conclusion can be drawn from inspection of Fig. 13. This figure shows the Helium concentration at probe 15 which was the farthest towards the center of the model. (See also Figs. 3a and 4). As can be seen, after some distance downstream the concentration of Helium starts increasing, showing the effect of the merging of the edges of adjacent jets. A similar effect, though on a reduced scale, can be observed in Fig. 14 which describes point 16.

Figure 15 describes the behavior at point 3 which was always centered on the nozzle. It was expected that this point will produce the highest concentrations and it did so in most cases. However, inspection of Tables 2-5 will show that in some instances this was not the case. The explanation of this phenomenon is as follows. The form of the concentration profile near the center is such that normally it contains a very pronounced peak. A very small movement of this peak from true center could change the reading by anything from 5 to 10%. Precise locating of this peak would have meant mapping of the flow in the vicinity of the center on a very fine grid at every location of the nozzle. While being of interest this would have entailed tremendous physical effort and expense.

Another interesting observation can be made as regards points 1, 6 and 8 (Figs. 16, 17 and 18, respectively). Inspection of these figures will

show that the concentration of Helium at point 8 is markedly lower than that at point 6. The effect is not so pronounced for point 1 but careful inspection will show that it is still true, namely that concentration at point 1 is lower than at point 6. All this holds at the lower X/D's. The effect evens out somewhat further downstream. It should be remembered that all these points, 1, 6 and 8, are equidistant from the nozzle center. The reason for this phenomenon is the lower mixing rate due to the slower flow between the nozzles. The strut, which may affect the flow field at the location of point 6, is too far upstream (more than 3 inner strut thicknesses) and its effect is weak in comparison.

In Fig. 19 the concentration is plotted against S/D. This was done for the points of maximum concentration. As mentioned before, the trends are not clear until about X/D of 24 or even 36. While some question could be cast about the validity of the up and down trends of some of these concentrations, a closer look will reveal that the general shape of the curves remains approximately the same from one X/D to the next. Since these results are based on different tests taken at different times it has to be concluded that they are valid and this behavior is the result of the local flow conditions as governed by the shape of the nozzles, the struts and the tunnel walls.

Finally, it is interesting to compare Figs. 12 and 15. These are the plots for the points of maximum concentration and for the concentration at the center of the nozzle. The graph in Fig. 12 behaves in a more orderly manner compared with the one in Fig. 15 and this amplifies the statement made previously concerning the movement of the peak of the jet and the jet itself, and validates the conclusion that these are the true maxima of the concentrations along the tunnel axis.

D. Mach Number Plots

The pressure readings obtained were converted into Mach number by the procedure described in Appendix D. The data presented consists of tables of Mach number for all points measured (Tables 7 - 10) and some representative graphs.

For each of the S/D values, pressure data were taken at six points. Three of these were with probe number 3 at the geometric center of the nozzle and at X/D of 0.1, 24 and 48. These will be later referred to as the "centered" measurements. The other three were at the same X/D's but with probe number 3 in the so-called "off-center" location. This was half-way between the upper and lower nozzles and 0.100" from the center of the model. Since this point was fixed relative to the tunnel, its distance from the nozzles changed with changing S/D. The exact location of the rake relative to the nozzles in the different S/D configurations is given in Fig. 4. This drawing should be kept in mind when analyzing the Mach number data.

The static probe, described previously in the section on instrumentation was located at the exact positions of probe number 3, both for the center and off-center readings.

Inspection of Fig. 20 will show that Mach number is effected less by distance downstream and considerably more by the distance between the nozzles, increasing with S/D. This result is as expected since by increasing S/D there is actually a smaller amount of blockage in the tunnel (the struts recede into the tunnel wall) and, more importantly, when the nozzles separate from each other some of the effects of interference diminish causing the flow to be less disturbed.

These results are shown again in Fig. 21. Here Mach number is plotted against S/D for X/D's of 24 and 48. The results are for point 9 which lies along a horizontal line through the center of the model and is located towards the inside. (See Figs. 3a and 4). As can be seen, the Mach number increases with S/D and the effect is more pronounced for X/D of 24 than for 48. This again is logical since at points far downstream all effects of variations in model configuration are evened out. It should be recalled that Helium concentration data, as effected by S/D, also became more regular at or about X/D = 36 (see Fig. 12, for example).

One more important aspect of Mach number calculations from the pressure measurements should be noted. Since the flow contains appreciable amounts

of Helium, the average γ of the flow is not 1.4 and the Mach number results, based on theoretical results in Ref. 18 and 19, would be affected. This, of course, will affect any calculation containing γ. A special calculation was made for the case of X/D of 24 and S/D of 1.5 which had the highest concentration of Helium. The case of X/D of 0.1, though containing more Helium, was not really valid because the flow coming out of the nozzle was expanding and results would have been inaccurate. Helium concentration at X/D of 24 was taken from the Gas Chromatograph data and equalled 22% and the new γ came to be 1.458. Based on this number, all data from Ref. 19 was recalculated and the new Mach numbers are given in Table 11. Unfortunately, there was no way to recalculate data from Ref. 18. This was, however, only an exploratory effort and the difference proved to be small, amounting to a maximum of 3.5% and this, as mentioned, at the highest Helium concentration for which M was calculated. It may be concluded that in most theoretical calculations these amounts of Helium will not introduce large mistakes and standard tables could be used, at least in a preliminary manner.

As a last conclusion, it may be noted that the final Mach number of the flow, far downstream, is about 2.9. Considering the initial conditions of the flow upstream of the injector (M = 4.0), this shows that one of the original design goals for this model, namely small disturbance to the flow, was achieved.

IV. THEORETICAL ANALYSIS

Concurrently with the experimental work the development of a theoretical analysis was undertaken in order to allow generalization of the experimental data and to provide a tool so that performance of injectors could be predicted, at least in a preliminary manner. A key restriction placed upon this effort was that the final product should be simple and easy to apply without the expenditure of a large amount of computer time for any given problem.

As a starting point for this analytical effort, the approximate mixing analysis of Libby (Ref. 20) was chosen. While retaining the original philosophy of this work, some modifications were made, based upon more current and better understanding of the mechanism of turbulent mixing and eddy viscosity modelling. Following the initial development in Ref. 20 we begin with the boundary-layer equations for axisymmetric flow written in Von Mises coordinates

$$u_x = \frac{1}{u_e \psi}\left(\left[\frac{\varepsilon \rho^2 r^2 u}{\rho_e^2 u_e \psi^2} \right] \psi u_\psi \right)_\psi \tag{1}$$

At this point Libby combined two operations, namely a transformation of $\rho^2\varepsilon$ to $\rho_o^2\bar{\varepsilon}$, where ρ_o is a reference density and $\bar{\varepsilon}$ is an "incompressible" eddy viscosity, and a linearization of the term in the parentheses on the right hand side of Eqn. (1). We choose to affect a linearization directly, leaving the compressive eddy viscosity intact. Thus take:

$$\frac{(\rho^2\varepsilon) r^2 u}{\rho_e^2 u_e \psi^2} \approx \frac{\rho\varepsilon}{\rho_e} A(x) \tag{2}$$

where A(x) is an, as yet unspecified, stretching factor to make the approximation in Eqn. (2) as reasonable as possible.

We proceed now

$$u_x = \frac{\rho\varepsilon A(x)}{\rho_e u_e \psi}\left(\psi u_\psi\right)_\psi \tag{3}$$

or introducing a new streamwise variable $\xi(x)$, defined as

$$\xi \equiv \int_o^x \frac{(\rho\varepsilon)\ A(x)}{\psi_j \rho_e u_e}\, dx \tag{4}$$

We get

$$u\xi = \frac{\psi_j}{\psi}\left(\psi u_\psi\right)_\psi \tag{5}$$

It is of considerable importance to note here that as this equation is linear, the solution for an arbitrary number and/or geometrical arrangement of injectors can be found from that for a single injector by simple algebraic superposition!

It remains now to specify a form for the eddy viscosity, select A(x) and write boundary conditions in order to complete the mathematical statement of the problem in terms of Continuity and Momentum equations. Solving this system will produce a solution for $u(\xi,\psi)$ which can be converted to $u(x,r)$. This leaves the temperature and concentration fields unknown. However, generalized crocco integrals can be used to relate these to the velocity field (20). Thus solving for $u(\xi,\psi)$ effectively completes the problem.

Rather than using the eddy viscosity model of Libby, we choose to model the eddy viscosity term by a more advanced one proposed by Schetz (Ref. 21). It has the advantage of being based on more recent developments in the study of turbulent mixing and, as will be shown shortly, makes theoretical calculations conform considerably better with experimental results.

Using the work by Schetz we write then

$$\rho\varepsilon = \frac{K_2\pi}{a}\int_o^\delta |\rho_e u_e - \rho u|\, 2r\, dr = \frac{K_2\pi}{a}\,\rho_e u_e\, |\delta^2 - \psi_\delta{}^2| \tag{6}$$

where ψ_δ corresponds to the value of ψ at the outer edge of the mixing region, $r = \delta$. Using then Eqn. (4) gives:

$$x = \frac{a\psi_j}{K_2\pi}\int_o^\xi \frac{d\xi}{A(\xi)|\delta^2 - \psi_\delta{}^2} \tag{7}$$

Before proceeding further the value of A(x) (or A[ξ(x)]) must be determined. It will be recalled that A(x) was defined in Eqn. (2) as

$$A(x) = \frac{\rho u r^2}{\rho_e u_e \psi^2} \tag{8}$$

Clearly the right hand side is actually a variable depending on distance from the injector nozzle center line, i.e., r. Moreover, r itself is a function of ψ as defined in Eqn. (8) in Ref. 20. Thus, a representation as a function of x alone can only be approximately correct. It can be shown that at x = 0, when going from the center of the nozzle outward, the value of A will tend to $\rho_j u_j/\rho_e u_e$ after starting with a value of 1.0 near the axis. Indeed, with a step type of initial profile

$$A = 1 \qquad\qquad r \leq a$$

$$A = \frac{\rho_j u_j}{\rho_e u_e} \qquad \frac{r^2}{\frac{\rho_j u_j}{\rho_e u_e} a^2 + (r^2 - a^2)} \qquad r \geq a \tag{9}$$

We will leave the quantity A(x) unspecified as yet and choose a simple

representation on the basis of comparison with experiment below. Suffice it to say here that we looked for and found a suitable form where A could be taken as a simple constant for any particular problem, not even a function of "x."

With all of this, the solution in the transformed plane (ξ,ψ) can be found as by Libby (20) in terms of Master's (Ref. 22) P function. Note here, however, that our definition of ξ differs from Libby's due to the difference in linearization and eddy viscosity models.

We are now in a position to return to specifying "A." For this purpose, consider the low speed, air-air experiments of Forstall and Shapiro (23). These were used as experimental reference and results of calculations using different methods are shown in Fig. 22 which includes the experimental data, Libby's prediction, a prediction obtained from an "exact" numerical solution using the Schetz eddy viscosity and two predictions from the present analysis depending on whether A is taken as simply unity or $A = \frac{\rho_j u_j}{\rho_e u_e} = 2.0$, which is its value as $r \to \infty$. All these results are for $\frac{\rho_j u_j}{\rho_e u_e} = 2.0$. The results are very encouraging in that with A = 1.0, excellent agreement with the data and the exact numerical solution is obtained. Note in particular that the rate of decay of the velocity excess (the slope of the curves in Fig. (22)) is predicted in much better agreement with the data than by the original Libby analysis. This is attributed to the more correct eddy viscosity model in use here.

We are encouraged now to compare the predictions of our analysis with the results of the present experiments. The initial profiles in the jet were taken as uniform with the one-dimensional average values of the flow variables. Such a comparison is given in Fig. 23 for S/D = 3.0 since this case has been shown to behave like an isolated jet.

The "free stream" of the experiment was approximated as a uniform stream with the following properties:

Mach numer	2.99	Total temperature	520°R

Total pressure	58.6 psia	Static pressure	1.6 psia
Static temperature	186°R	Velocity	2001 ft/sec
Density	0.023 lbs/cu ft		
Reynolds number, based on strut's chord (2.0 inches)			783000

As can be seen, the theoretical results conform well with experimental results. The experimental results for X/D of 1 and 3 were omitted altogether because, as mentioned earlier when discussing experimental results, there is an "inversion" in results which must be attributed to the presence of the injector itself and its effect on the flow. Such effects cannot be treated by an analysis of this type. The two analytical curves correspond to A equal unity and A = 0.3901, since in this case $\frac{\rho_j u_j}{\rho_e u_e}$ equals 0.3901. As before, the smaller value of A provides the most accurate prediction. As can be seen, in this case too, agreement between calculation and experiment is very good.

On this basis, we suggest the following simple rule for selection of A: The value of A should be chosen as unity or $\rho_j u_j / \rho_e u_e$, whichever is smaller.

So far, all the calculations were concerned with the prediction of conditions on the center line. Next, an attempt was made to compare theoretical calculations with experiment at points off the center. The results of this comparison are presented in Figs. 24 and 25. In Fig. 24 concentration profiles are presented against nozzle geometry for different X/D's (comparable to Figs. 8 to 10). Both theoretical and experimental results are given and as can be seen the agreement is very good up to a distance equal to a nozzle's radius from the center line, and then the experimental results drop off more sharply than the prediction. The reason for this discrepancy can be traced to the fact that we assumed an eddy viscosity which is constant across the whole mixing region, and clearly this is not the case. Some type of "intermittency" distribution as a function of radial distance would be more appropriate. The correlation between test and theory does improve slightly at X/D of 48 but this is probably due to the fact that at that distance downstream adjacent Helium jets start merging. Figure 25 shows the effect

of X/D on Helium concentration for different distances from the nozzle centerline. Again, the fact that the results conform best nearer to the centerline is clearly visible.

Since the comparison between analysis and experiment deteriorates at the outer edge of the mixing region, the effects of adjacent jets can only be accurately calculated with the present analysis for "strong merging" cases, i.e., where the effect of adjacent jets penetrates to within roughly one or two jet radii from the center. However, these are exactly the cases of primary interest from a practical standpoint, since only for such cases can the concentration in the major part of the mixing field be modified. The prediction for the centerline concentration for all experimental cases (i.e., S/D = 1.5, 2.0, 2.5 and 3.0) are shown in Fig. 26 in which the following points should be noted: injectant concentration depends on S/D up to S/D of 2.5 both for theory and experiment; the rate of change of the concentration as a function of S/D is similar for experimental results and theoretical calculation; the agreement between theory and experiment is also good for the absolute values of the concentration. It is important to note that all these calculations were done by hand using only a desk calculator. With a little experience, an engineer can produce a prediction for a two fluid, high Mach number case in about 15 hours.

V. DISCUSSION

The results of an experimental and analytical investigation of a strut mounted, downstream facing, multiple nozzle Helium injector were described in this report. The main parameter varied was the interjet spacing (S/D), and gas analysis data and pressure (and Mach No.) surveys were obtained for four S/D's at seven axial stations. In addition, Schlieren pictures were obtained for most of the runs.

Results indicate that S/D has an influence both on injectant concentrations and Mach No., with concentration decreasing and Mach No. increasing with increasing S/D. The effect on concentrations, however, was felt only up to S/D of 2.5. It was noticed also that in regions of lower flow velocity, mixing was retarded. Mach number data indicate that losses in Mach number, and consequently in total pressure, due to the strut, were not excessive, with Mach number dropping to approximately 3.0 from its free stream level of 4.0. This conclusion is corroborated, for the whole flow field, by the absence of strong shock waves on the Schlieren pictures.

The analytical method developed enables relatively quick and accurate prediction of the concentration of the injectant. Being linear it also provides prediction of the performance of arbitrary multi-nozzle arrangements by superposing results from single jets. Results of the analytical calculation show good agreement with experiment both for absolute values of the concentration and the effects of S/D on it.

APPENDIX A

ERROR ANALYSIS

The following discussion concerns the maximum probable error in results evolving from experimental data or combinations of experimental data and use of standard tables.

He Concentration

As mentioned, the vacuum pump could pump the cart down to 400 Millitorrs. During a run the bottles were filled to about 10" Hg absolute. Assuming the bottles contained pure air before the run, this will introduce a maximum error of -0.16% in Helium concentration.

A second source of error was the K factor used in Gas Chromatograph data reduction (see Appendix C). As shown elsewhere, this could lead to a mistake of not more than ±0.2% in any sample.

The Gas Chromatograph output was not linear with the actual Helium concentration. A calibration curve was prepared and rechecked several times but it is estimated that a ±0.5% error was possible in preparation and reading of this calibration curve.

When checking Helium concentration at a point which should have given 100% He, readings of no more than 96% could be obtained. Reasons for this were explained in the section on gas analysis data. The conclusion is that uncontrolled sources of contamination could reduce actual readings by 3-4%.

Based on these estimates, the readings of Helium concentration should be interpreted as meaning "concentration $^{+4\%}_{-0.7\%}$." It should be noted that since many times the total Helium concentration is given in percent, this is a possible source of confusion and the error should be understood as percent of the concentration and not percent added to the concentration.

There is no direct way to estimate the effect of small changes, $^{+1.6\%}_{-1.3\%}$,

in flow rate on the concentration readings. Based, however, on few analyzed runs for which later it was found that flow rates were slightly beyond these limits, it is believed that the effect is negligible.

Mach Number Data

It is estimated that the measured Pitot and cone-static pressures are within ±2% of their actual values. This number is based on the following possible errors. First, nonlinearity in the output of the transducers and errors in readings the strip charts. Further it is estimated that readings of additional charts used in computations will introduce additional ±1% error.

Since there are appreciable amounts of Helium in the flow, some computations were repeated using a corrected γ (C_p/C_v). Results are tabulated in Table 11. The results indicate that Mach number is probably in error by a maximum of 3.5%. This figure is not final because data from one of the references (Ref. 18) could not be directly corrected for γ. It may be concluded, bearing this inaccuracy in mind, that Mach number data for X/D = 24 is accurate to within $^{+3.0\%}_{-6.5\%}$. For X/D = 48 and for X/D = 0.1, where the measurements were taken in low Helium concentration flow, the Mach number data is correct to within ±3.0%.

APPENDIX B

9" x 9" SUPERSONIC WIND TUNNEL

The V.P.I. & S.U. 9 x 9 in. supersonic wind tunnel was designed and originally constructed at the Langley Aeronautical Laboratory. In 1958 the tunnel was purchased by V.P.I. & S.U. and, after being re-constructed in a specially designed building, was put into operation in 1963. During recent years several modifications were introduced into the air pumping, tunnel control, and instrumentational equipment which increased capabilities of the facility.

The facility is of an intermittent, blow-down type with interchangeable contoured nozzles. The air pumping system consists of eight Ingersoll Rand, Model 90, reciprocating compressors, of 800 hp total capacity. They can pump the storage system up to 150 psig. A very efficient drying and filtering system is provided which includes both drying by cooling and drying by absorption. The latter is accomplished by a fully automated system fabricated by the Kamp Co. and uses molecular sieves and activated alumina as desiccant. Air storage system consists of 16 tanks with a total volume of 2800 ft^3. Tunnel control system includes a quick opening butterfly valve and a pressure regulating system.

The settling chamber contains a perforated transition cone, several damping screens and probes measuring stagnation pressure and temperature. The nozzle chamber is interchangeable with two-dimensional contoured nozzle blocks made of steel. The tunnel is equipped with three complete nozzle chambers which presently are fitted with the nozzles for the Mach numbers 2.4, 3, and 4. Several other nozzle blocks are available (not calibrated).

The working section of the tunnel is equipped with a remotely controlled model support which allows one to vary the position of a model in the vertical plane.

An arrangement for side wall model mounting is also available. An extractable mechanism can be provided for supporting the model during the starting and stopping of the flow. Due to large windows in the nozzle and working sections, a very good access to the model is ensured.

After passing through a diffuser, the air flow is discharged into the atmosphere outside of the building.

Technical Specification of the tunnel:

Test Section size	9 x 9 inches
Stagnation pressure	40 - 120 psia
Mach number	2.4 - 4
Reynolds number per foot	6×10^6 to 15×10^6
Run duration, depending on Mach number	10 - 90 sec.
Maximum model diameter at M = 3	3.5 in.
Storage tank volume	2800 ft^3
Maximum air pressure in the storage tanks	150 psig
Total power rate of the compressor plant	800 hp

APPENDIX C

GAS ANALYSIS METHOD

Following collection of the samples in the gas collection cart shown in Fig. 5, the bottles were pressurized with Argon to about 50 psig. Since Argon was used as the carrier gas in the chromatograph, this dilution of the sample by the pressurization process had no effect on the sample.

To insert a sample into the chromatograph, a bottle was connected to the sample valve and opened to let a sample, mixed with Argon, flow through and purge the line. Then the sample valve was rotated, and the sample was run through the column and detector cell. The columns were made by the Bendix corporation and filled with Chromosorb 102. The output was read simultaneously on a Beckman 10" recorder and an Autolab 6300 digital integrator. All calculations of Helium concentration are based on integrator output which, compared with manual data reduction from the recorder output was considerably quicker, more consistent and could accommodate the full spectrum of concentrations without the necessity of switching ranges.

The actual concentrations were calculated according to the following procedure as suggested in Ref. 24. Complete details and justification for the procedure are available in the reference. The sample loop in the sample valve used was of 0.1 ml volume. The weights of 0.1 ml of pure air and Helium at atmospheric pressure were calculated. A pure sample of each gas was run through the chromatograph and the ratio of the outputs of Helium and air was multiplied by the ratio of actual weights of air and Helium. This gave a "K" factor for air. This was corrected to correspond to N_2, which was actually used in the procedure. Finally, the true mass percentage was obtained using

$$\frac{(\text{He output})}{(\text{He output}) + (N_2 \text{ output}) \times K} \cdot 100 = \% \text{ He in sample}$$

The factor K was recalculated before each batch of samples because of the possibility of drift in the electronic system of the integrator. It was found to be steady within less than ±0.2%. Since the K factor operated only on one of the constituents, air, the error in concentration was even smaller depending on relative amounts of air and Helium.

In order to further ensure reliability of results obtained by the Gas Chromatograph, each sample was run at least twice through the instrument and unless results were within 2 percent of each other (namely ±1.0%) the same sample was rerun until at least two runs came within this range. In most cases there was no need for the third run. Occasionally, notably with high Helium concentration samples, a third run was required and rarely a fourth. The reason that this occurred mostly at high Helium concentration is due to the fact that Argon was used as carrier gas in our tests, and under these conditions both Nitrogen and Oxygen gave an extremely small signal compared with Helium.

APPENDIX D

MACH NUMBER CALCULATION PROCEDURE

To determine the Mach number from the Pitot and static pressures the following procedure is employed. First, the ratio of the cone static pressure to the Pitot pressure at point 3 is determined. It should be recalled that the static pressure was measured always at the same point 3. This ratio may be expressed as

$$\frac{P_c}{P_{t_2}} = \frac{P_c}{P_\infty} \frac{P_1}{P_{t_1}} \frac{P_{t_1}}{P_{t_2}}$$

Now the quantity P_c/P_{t_2} is obtained from Ref. 18 and plotted against Mach number. The other two ratios, namely P_1/P_{t_1} and P_{t_1}/P_{t_2} are obtained from Ref. 19. Actually, the value of P_1/P_{t_2}, which is the one we are really looking for, is tabulated itself in Ref. 19. A plot of this value is now made against Mach number, and it is advantageous to have both plots on the same chart. Now the ratio P_c/P_{t_2} for point 3 is used to find Mach number on the first plot. This is actually the Mach number at point 3. Next, at this Mach number, the value of P_1/P_{t_2} is read from the second plot and multiplied by the total (Pitot) pressure of point 3. This gives P_1 which we may assume is constant across the mixing region. By dividing the values of the Pitot pressure at the different probes into this P_1 we obtain the appropriate values of P_1/P_{t_2} at the different probe locations. These values are now converted to Mach numbers by the second plot, that of P_1/P_{t_2}.

It should be recalled that all references cited are for air ($\gamma = 1.4$). Since the flow contained appreciable amounts of Helium (22% at X/D of 24), the tables from Ref. 19 were recalculated using the new γ (1.458) and it was found that the Mach number was reduced, but never by more than 3.5%. (See Table 11)

REFERENCES

1. Weber, R. J. and Mackay, J. S., "An Analysis of Ramjet Engines Using Supersonic Combustion," NACA TN 4386, Sept. 1958.

2. Dugger, G. L., "Comparison of Hypersonic Ramjet Engines with Subsonic and Supersonic Combustion," Combustion and Propulsion, Fourth AGARD Colloquim, High Mach Number Air-Breathing Engines, A. L. Jaumotte, A. H. Lefebvre, A. M. Rothrock, Editors, Pergamon Press, New York, 1961, pp. 84-110.

3. Avery, W. H. and Dugger, G. L., "Hypersonic Airbreathing Propulsion," Astronautics and Aeronautics, June 1964, pp. 42-47.

4. Longwell, J. P., "Combustion Problems in Ramjets," Fifth Symposium (International) on Combustion, Combustion in Engines and Combustion Kinetics, Reinhold Publishing Corp., New York, 1955, pp. 48-56.

5. Cohen, L. S., Coulter, L. J., and Egan, W. J., Jr., "Penetration and Mixing of Multiple Gas Jets Subjected to a Cross Flow," AIAA Journal, Vol. 9, No. 4, April 1971, pp. 718-724.

6. Burnett, D. R. and Czysz, P., "Supersonic Hydrogen Combustion Studies," ASD-TDR-63-196, Air Force Systems Command, Wright-Patterson AFB, April 1963.

7. Kush, E. A., Jr. and Schetz, J. A., "Decomposition of a Liquid Jet Injected Normal to a Supersonic Air Stream," VPI-E-10-72, June 1972, AFOSR Scientific Report AFOSR-TR-72-1180.

8. Swithenbank, J. and Parsons, R. J., "Experimental Techniques for Supersonic Combustion Research in a Shock Tunnel," 30th Propulsion and Energetics Panel Meeting on "New Experimental Techniques in Propulsion and Energetics Problems," Report No. H. I. C. 95, Department of Fuel Technology and Chemical Engineering, University of Sheffield, Sheffield, England.

9. Ferri, A., Libby, P. A., and Zakkay, V., "Theoretical and Experimental Investigation of Supersonic Combustion," High Temperatures in Aeronautics, Pergamon Press, New York, September 1962, pp. 55-118.

10. Billig, F. S., "Supersonic Combustion of Storable Liquid Fuels in Mach 3.0 to 5.0 Air Streams," Tenth Symposium (International) on Combustion, The Combustion Institute, Pittsburgh, Pa., 1965, pp. 1167-1178.

11. Abramovitch, G. N., The Theory of Turbulent Jets, MIT Press, Cambridge, Mass., 1963.

12. Schetz, J. A., "Unified Analysis of Turbulent Jet Mixing," NASA CR-1382, July 1969.

13. Harsha, P. T., "Free Turbulent Mixing: A Critical Evaluation of Theory and Experiment," AEDC TR-71-36, February 1971.

14. Proceedings of the NASA Workshop on Free Turbulent Flows, NASA SP-321, Vol. 1 Conference Proceedings; Vol. 2 Summary of Data, July 1972.

15. Lorber, A. K. and Schetz, J. A., "Turbulent Mixing of Multiple, Co-Axial Helium Jets in a Supersonic Airstream, NASA CR-112292, March 1973.

16. ASME Power Test Codes, Part 5, Measurement of Quantity of Materials, Chapter 4, Flow Measurements, American Society of Mechanical Engineers, New York, 1959.

17. Keenan, J. H. and Kaye, J., Gas Tables, John Wiley & Sons, Inc., New York, 1948.

18. Sims, J. L., Tables for Supersonic Flow Around Right Circular Cones at Zero Angle of Attack, NASA SP-3004, 1964.

19. Anon., Equations, Tables and Charts for Compressible Flow, NACA Report 1135, 1953.

20. Libby, P. A., "Theoretical Analysis of Turbulent Mixing of Reactive Gases with Application to Supersonic Combustion of Hydrogen," ARS Journal, Vol. 32, No. 3, March 1962, pp. 388-396.

21. Schetz, J. A. "Turbulent Mixing of a Jet in a Coflowing Stream," AIAA Journal, Vol. 6, No. 10, October 1968, pp. 2008-2010.

22. Masters, J. I., "Some Applications in Physics of the P Function," The Journal of Chemical Physics, Vol. 23, No. 10, October 1955, pp. 1865-1874.

23. Forstall, W., Jr. and Shapiro, A. H., "Momentum and Mass Transfer in Coaxial Gas Jets," Journal of Applied Mechanics, Vol. 17, 1950, pp. 399-408.

24. McNair, H. M. and Bonelli, E. J., Basic Gas Chromatography, Varian Aerograph, Walnut Creek, California, 1969.

Table 1

Listing of Timer Functions and Timings

Time (seconds)	Operation
0	Start timer
0.5	Start recorders
0.5	Start Helium
0.5	Start tunnel
3.5	Start sample
5.0	Take picture
6.5	End sample
7.0	Stop Helium
7.0	Stop tunnel
8.0	Stop recorders

TABLE 2

HELIUM CONCENTRATION (MASS FRACTION, %, He) TABULATION,

S/D = 1.5

	Probe No.													
X/D	1	2	3	4	5	6	8	9	10	11	15	16	17	18
1	56.5	59.5	68.0	38.0	33.0	53.5	17.5	26.5	58.0	69.0	1.2	1.1	63.0	39.0
3	9.5	63.0	74.5	36.0	33.0	53.5	10.0	34.0	60.5	53.0	3.0	2.8	35.0	25.5
6	10.0	54.5	51.5	34.5	28.0	38.0	10.5	31.0	43.5	34.5	2.4	2.6	24.0	22.0
12	18.5	27.0	27.1	20.0	21.0	2.5	5.0	16.5	32.0	23.5	2.2	4.0	26.5	14.0
24	11.0	22.5	21.6	19.3	17.0	21.0	16.5	15.0	18.5	20.8	9.0	9.0	15.7	15.0
36	9.0	17.0	15.5	17.0	14.0	17.0	9.0	14.0	16.5	12.5	18.5	16.5	16.7	10.0
48	7.2	12.5	12.2	13.2	10.5	12.5	5.5	12.0	14.0	10.0	15.0	12.5	14.0	8.0

TABLE 3

HELIUM CONCENTRATION (MASS FRACTION, %, He) TABULATION,

S/D = 2.0

	Probe No.													
X/D	1	2	3	4	5	6	8	9	10	11	15	16	17	18
1	27.0	48.5	60.5	30.3	16.8	56.8	10.0	51.0	6.6	61.0	1.7	1.0	58.0	45.7
3	5.5	44.0	58.6	34.8	34.3	27.0	4.6	18.0	10.8	45.5	1.0	1.7	18.9	14.0
6	10.0	49.4	56.7	35.0	30.8	41.7	9.0	35.0	10.5	63.6	3.0	2.1	23.5	9.5
12	13.0	27.5	28.6	27.4	24.7	22.0	6.0	18.5	7.0	16.5	1.0	12.5	29.2	15.0
24	5.5	15.0	16.0	14.0	13.2	15.1	5.0	10.0	3.5	14.8	2.2	6.0	11.5	12.5
36	6.4	10.5	12.6	12.2	12.5	13.5	5.5	10.7	4.0	10.4	7.0	8.6	11.8	9.0
48	4.8	8.0	9.0	9.0	8.8	9.0	3.6	8.1	2.3	7.0	8.5	8.5	10.5	7.0

TABLE 4

HELIUM CONCENTRATION (MASS FRACTION, %, He) TABULATION,

S/D = 2.5

	Probe No.													
X/D	1	2	3	4	5	6	8	9	10	11	15	16	17	18
1	47.5	65.7	52.3	24.4	36.0	59.0	17.0	44.4	7.0	39.5	2.0	2.4	52.5	40.7
3	33.0	67.3	72.3	37.0	35.6	53.2	13.4	39.5	56.5*	70.8	2.6	3.7	38.0	11.8
6	27.5	20.8	71.1	30.6	25.8	39.5	7.8	55.5	30.0*	51.2	2.0	3.2	36.8	5.2
12	47.0	21.7	20.0	18.0	21.9	19.7	9.0	42.8	12.0*	11.5	2.2	16.4	35.5	13.0
24	12.0	17.0	18.8	13.0	2.0**	11.3	5.2	15.2	15.1*	15.0	1.5	3.7	11.5	10.3
36	6.4	8.3	10.0	8.3	4.5**	9.0	5.2	7.2	9.0*	9.0	2.2	3.6	7.3	7.2
48	5.6	7.0	6.5	6.3	5.0**	6.8	5.8	7.2	7.6*	7.5	3.6	4.2	7.5	6.6

* These readings are for Probe No. 12 instead of No. 10

** These readings are for Probe No. 7 instead of No. 5

TABLE 5

HELIUM CONCENTRATION (MASS FRACTION, %, He) TABULATION,

S/D = 3.0

	Probe No.													
X/D	1	2	3	4	5	6	8	9	10	11	15	16	17	18
1	31.8	52.0	53.0	42.5	26.0	49.5	13.5	49.0	58.5	46.0	1.2	1.4	56.5	45.0
3	33.0	68.0	66.0	56.0	43.0	46.0	11.0	36.3	58.0	58.8	1.0	3.0	35.5	15.9
6	16.4	67.5	63.6	35.2	28.5	39.8	8.6	34.0	51.0	36.7	1.0	2.0	31.0	6.2
12	24.3	22.0	14.5	12.0	15.0	25.0	8.0	33.5	28.8	8.6	0.7	9.5	40.0	7.5
24	9.0	15.5	18.3	14.9	11.0	8.0	4.5	12.8	17.0	15.7	0.5	3.8	12.4	12.3
36	5.2	8.2	10.2	8.8	8.6	7.7	4.1	7.4	10.0	9.3	0.9	9.8	7.0	8.2
48	5.0	6.7	7.2	6.9	6.7	6.4	4.2	5.2	6.8	7.0	1.5	3.0	5.4	6.1

TABLE 6

He CONCENTRATIONS AT X/D = 0.1, S/D = 3.0

			Vertical Plane				
Probe No.*	1	2	3	4	5	6	7
Concentration (% He)	25.5	51.5	90.0	88.5	76.5	23.0	5.0
			Horizontal Plane				
Probe No.	1	2	3	4	5	6	7
Concentration (% He)	51.0	90.0	91.0	91.5	91.5	38.0	4.0

*In this test another rake, with different spacing of probes, was used. See Fig. 11.

TABLE 7

MACH NO. TABULATION, S/D = 1.5

Probe No.	X/D					
	0.1_A*	0.1_B**	24_A	24_B	48_A	48_B
3		2.42	2.07	1.91	2.05	2.16
8		2.48	1.77	1.56	2.54	2.68
9		2.53	2.02	1.95	2.02	2.08
10		2.52	2.03	1.94	2.04	2.09
11		2.46	2.05	1.89	2.12	2.17
12		2.76	2.07	1.89	2.10	2.18
13		2.77	2.07	1.90	2.11	2.19
14			2.07	1.91	1.98	2.19
15	1.38		2.08	1.92	1.97	2.19
16	1.38	2.37	2.09	1.90	1.98	2.14
17		2.54	2.03	1.93	2.00	2.15
18			2.04	1.89	2.05	2.15
19			2.08	1.89	2.06	2.16

*A denotes Probe 3 centered on nozzle 3

**B denotes rake in off-center position as depicted in Fig. 4

TABLE 8

MACH NO. TABULATION, S/D = 2.0

Probe No.	X/D					
	0.1_A*	0.1_B**	24_A	24_B	48_A	48_B
3		3.36	2.69	3.28	2.53	2.87
8		3.42	2.64	3.66	2.40	2.42
9		3.58	2.65	3.84	2.40	2.82
10		3.52	2.67	3.66	2.57	2.83
11		3.23	2.71	2.98	2.58	2.85
12		3.23	2.72	2.91	2.63	2.85
13		3.23	2.72	2.84	2.64	2.88
14			3.57	2.84	2.56	2.89
15	4.00	3.28	3.52	2.93	2.57	2.89
16	3.92	3.34	2.88	3.30	2.58	2.89
17		3.48	2.69	3.72	2.58	2.82
18		3.34	2.69	2.90	2.60	2.84
19			2.72	2.85	2.62	2.88

* A denotes Probe 3 centered on nozzle 3

** B denotes rake in off-center position as depicted in Fig. 4

TABLE 9

MACH NO. TABULATION, S/D = 2.5

Probe No.	X/D					
	0.1_A*	0.1_B	24_A**	24_B***	48_A	48_B
3			1.95	3.74	2.40	2.83
8			1.45	3.32	1.33	1.28
9			1.94	3.84	2.34	2.76
10			2.51	3.25	2.64	2.86
11			1.91	3.58	2.31	2.76
12			1.94	3.41	2.31	2.68
13			2.02	2.87	1.45	1.30
14			3.08	2.46	2.56	2.51
15			3.03	2.98	2.42	2.62
16			1.96	3.66	2.34	2.65
17			1.91	3.72	2.28	2.80
18				3.19		2.65
19				3.02		2.62

* Results for X/D = 0.1 are unavailable due to failure to obtain static pressure readings

** A denotes Probe 3 centered on nozzle 3

*** B denotes rake in off-center position as depicted in Fig. 4

TABLE 10

MACH NO. TABULATION, S/D = 3.0

Probe No.	X/D					
	0.1_A*	0.1_B**	24_A	24_B	48_A	48_B
3		3.44	2.02	3.46	2.52	3.12
8		3.31	2.29	3.57	2.57	3.10
9		3.31	2.00	3.51	2.52	3.14
10		3.26	2.01	3.49	2.51	3.16
11		3.20	2.02	3.49	2.51	3.02
12		3.18	2.02	3.51	2.51	2.88
13		3.31	2.03	3.57	2.48	2.75
14		3.18	2.90	3.12	2.99	2.82
15	2.82	3.16	2.78	3.57	2.74	3.08
16	2.68	3.36	2.24	3.57	2.58	3.21
17		3.33	2.02	3.51	2.53	3.24
18		3.24	2.04	3.49	2.18	2.76
19		3.18	2.04	3.49	2.49	2.78

* A denotes Probe 3 centered on nozzle 3

** B denotes rake in off-center position as depicted in Fig. 4

TABLE 11

COMPARISON OF FLOW MACH NO. CALCULATED

USING $\gamma = 1.4$ and $\gamma = 1.458$

X/D = 24, S/D = 1.5, CENTERED

Probe No.	$M_\gamma = 1.4$	$M_\gamma = 1.458$
3	2.07	2.00
8	1.77	1.75
9	2.02	1.97
10	2.03	1.98
11	2.05	1.99
12	2.07	2.00
13	2.07	2.00
14	2.07	2.01
15	2.08	2.03
16	2.09	2.04
17	2.03	1.98
18	2.04	1.98
19	2.08	2.02

FIGURES

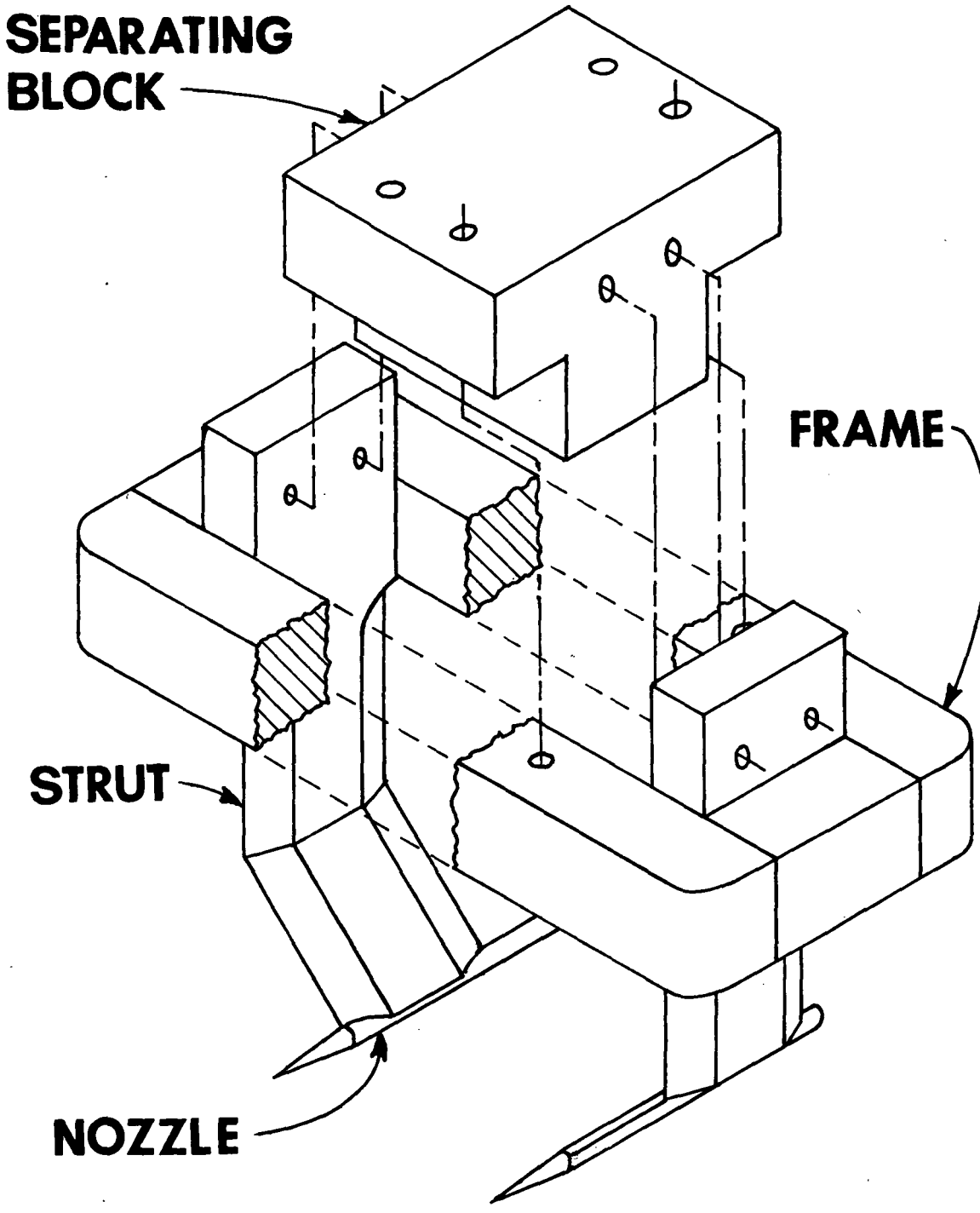

FIG. 1-A AN EXPLODED VIEW OF THE INJECTOR MODEL

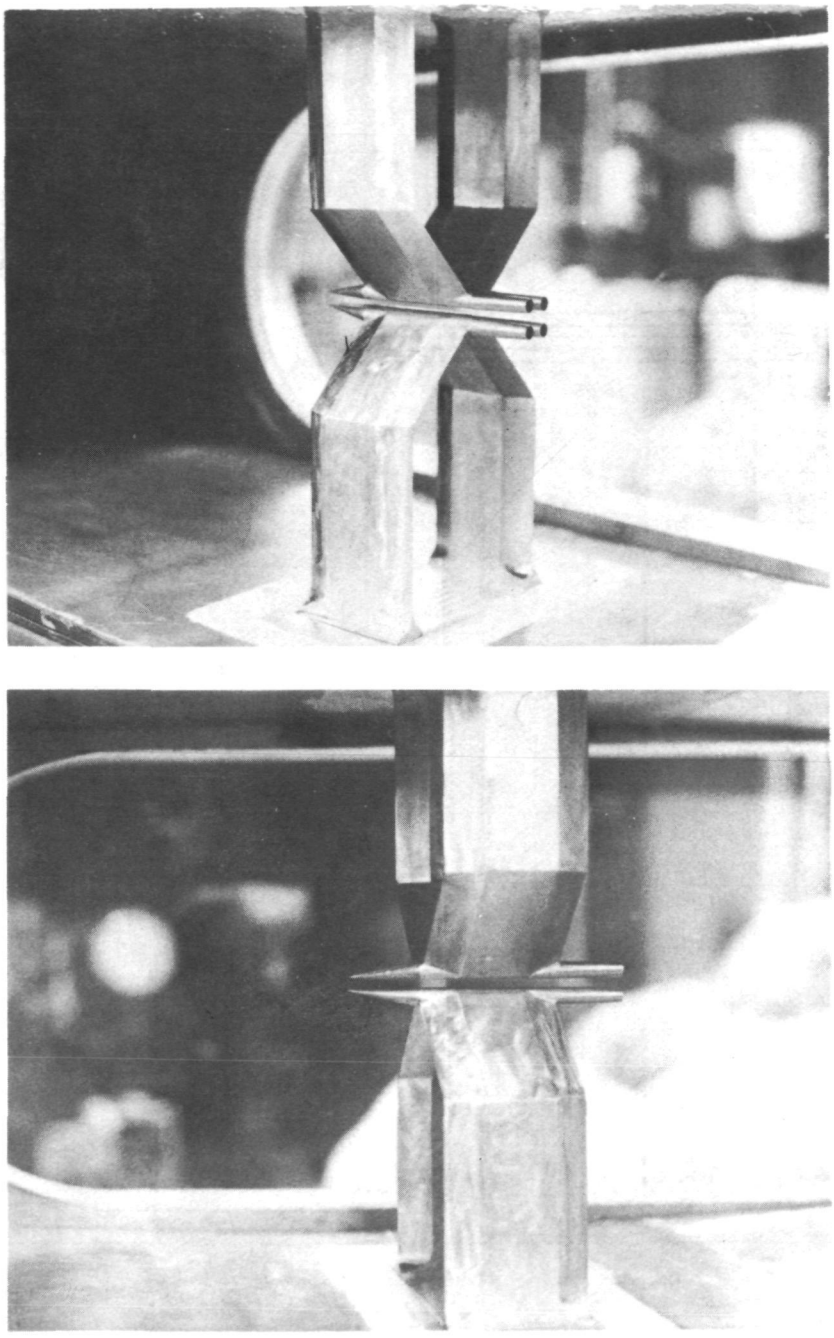

FIG.1-B PHOTOGRAPHS OF THE INJECTOR MODEL

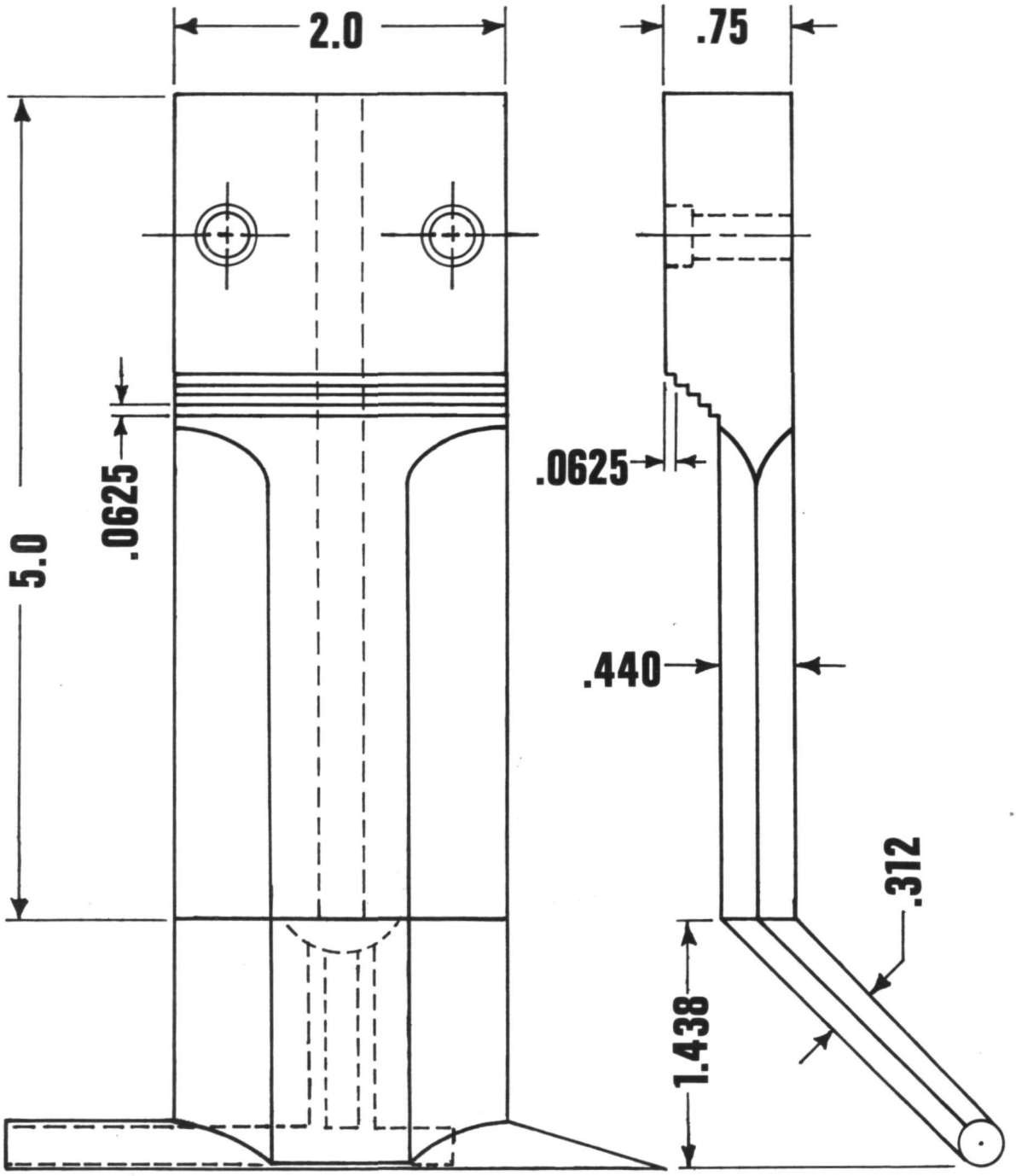

FIG. 1-C
DRAWING OF STRUT AND NOZZLE

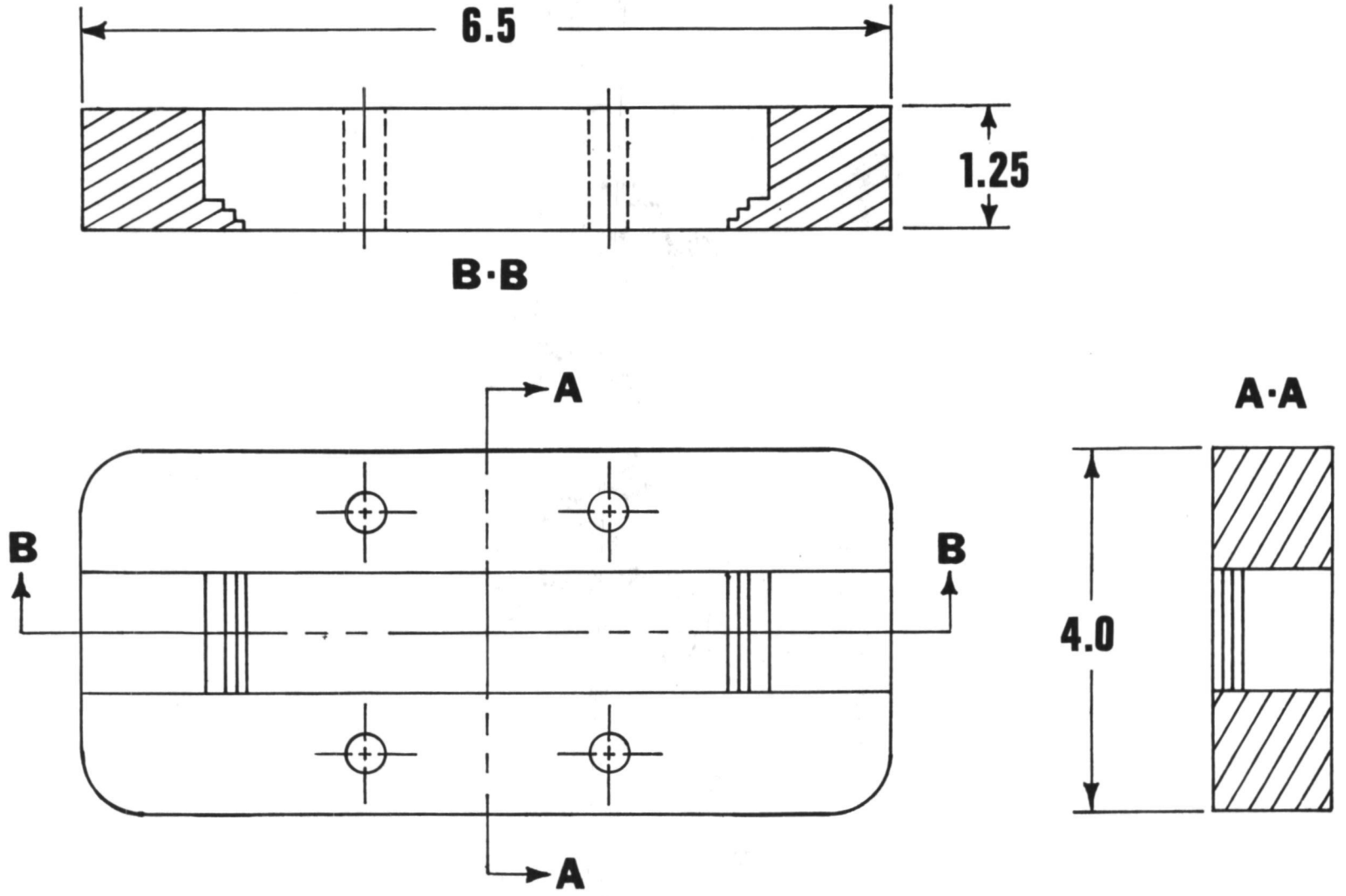

FIG.1-D STRUT SUPPORT FRAME

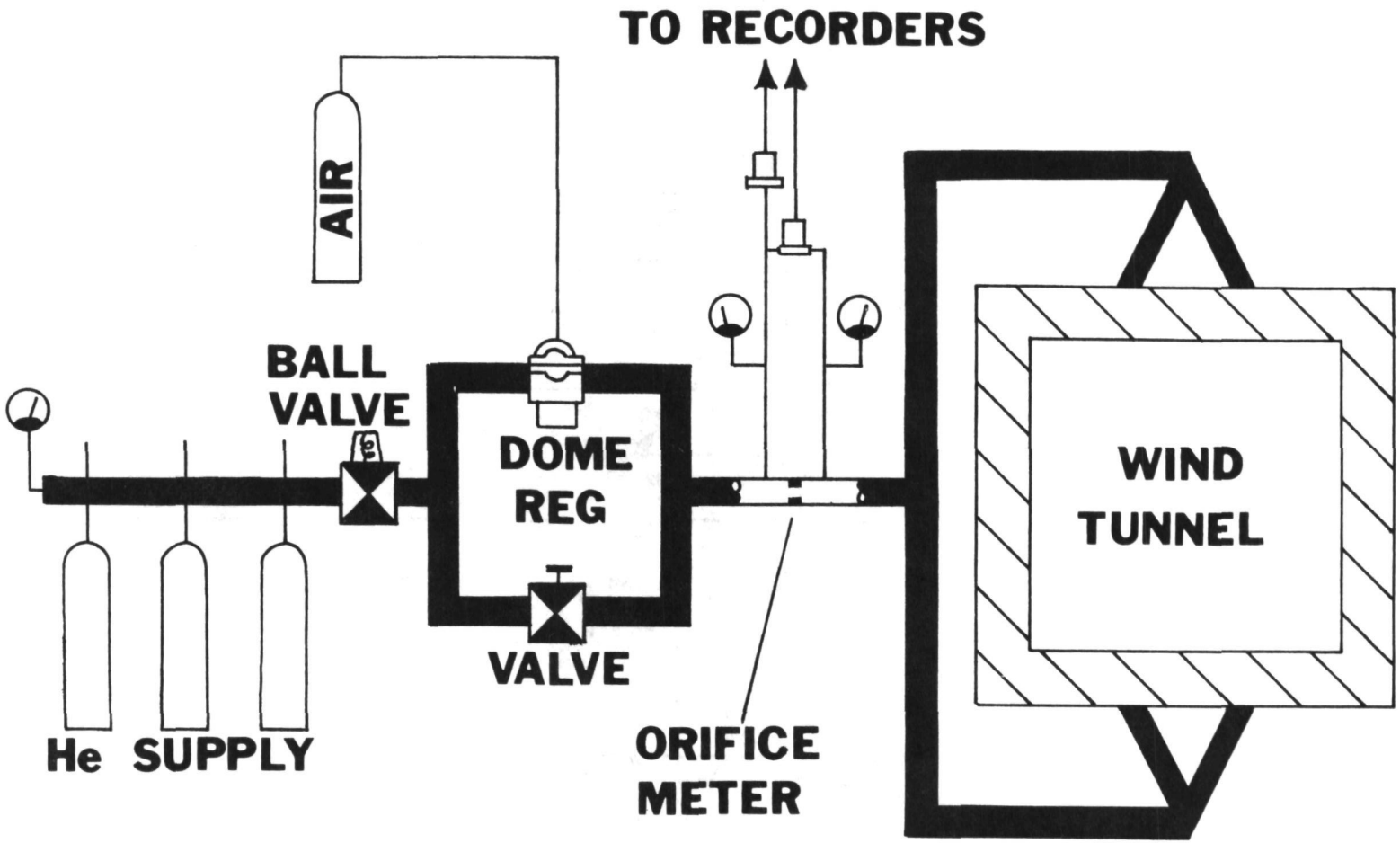

FIG. 2
SCHEMATIC DIAGRAM OF INJECTION SYSTEM

NUMBERS BETWEEN PROBES INDICATE SPACING IN THOUSANDTHS OF AN INCH, NO NUMBER INDICATES .050 INCH

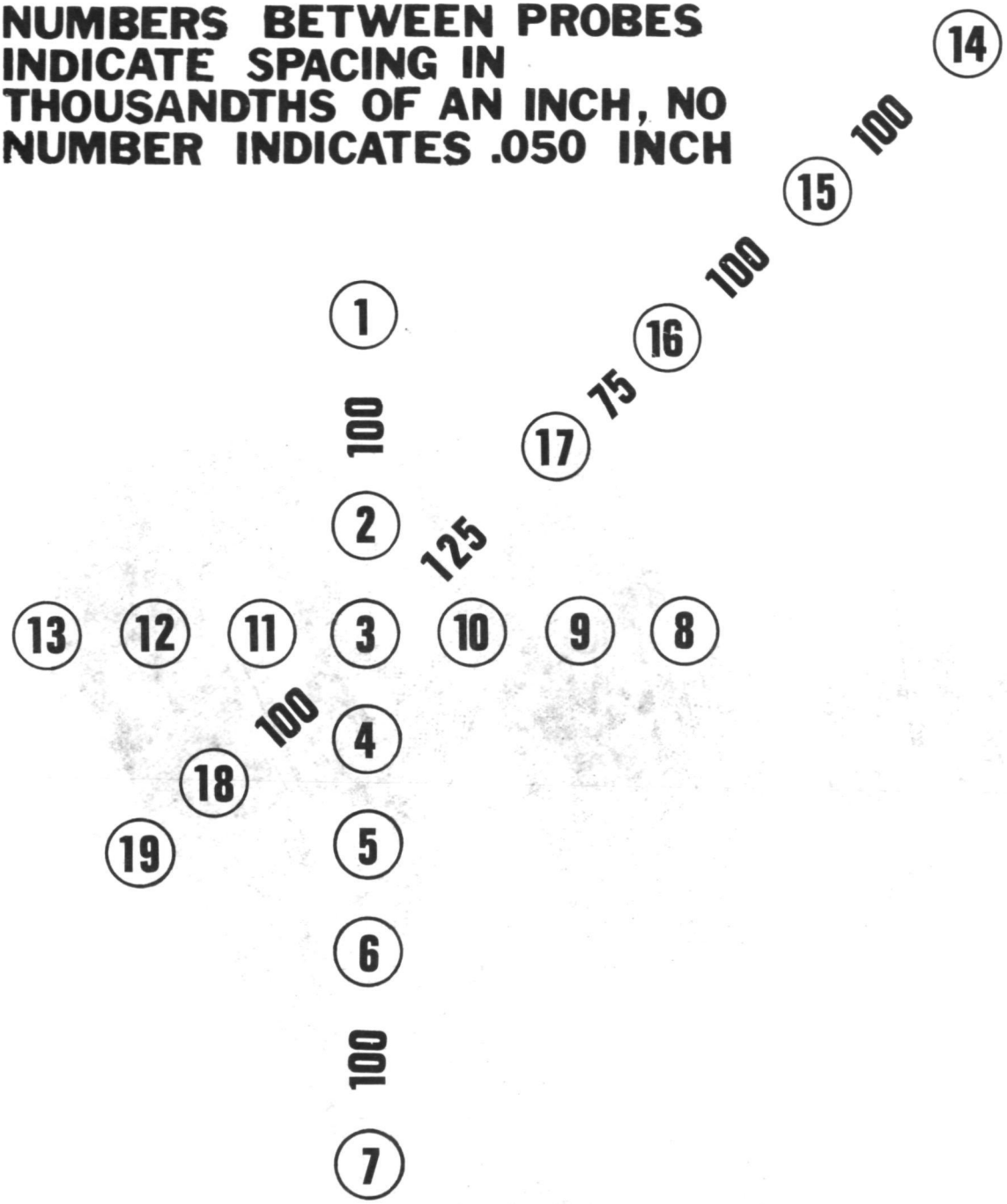

FIG 3-A

SCHEMATIC HEAD-ON VIEW OF THE RAKE WITH PROBE NUMBERS

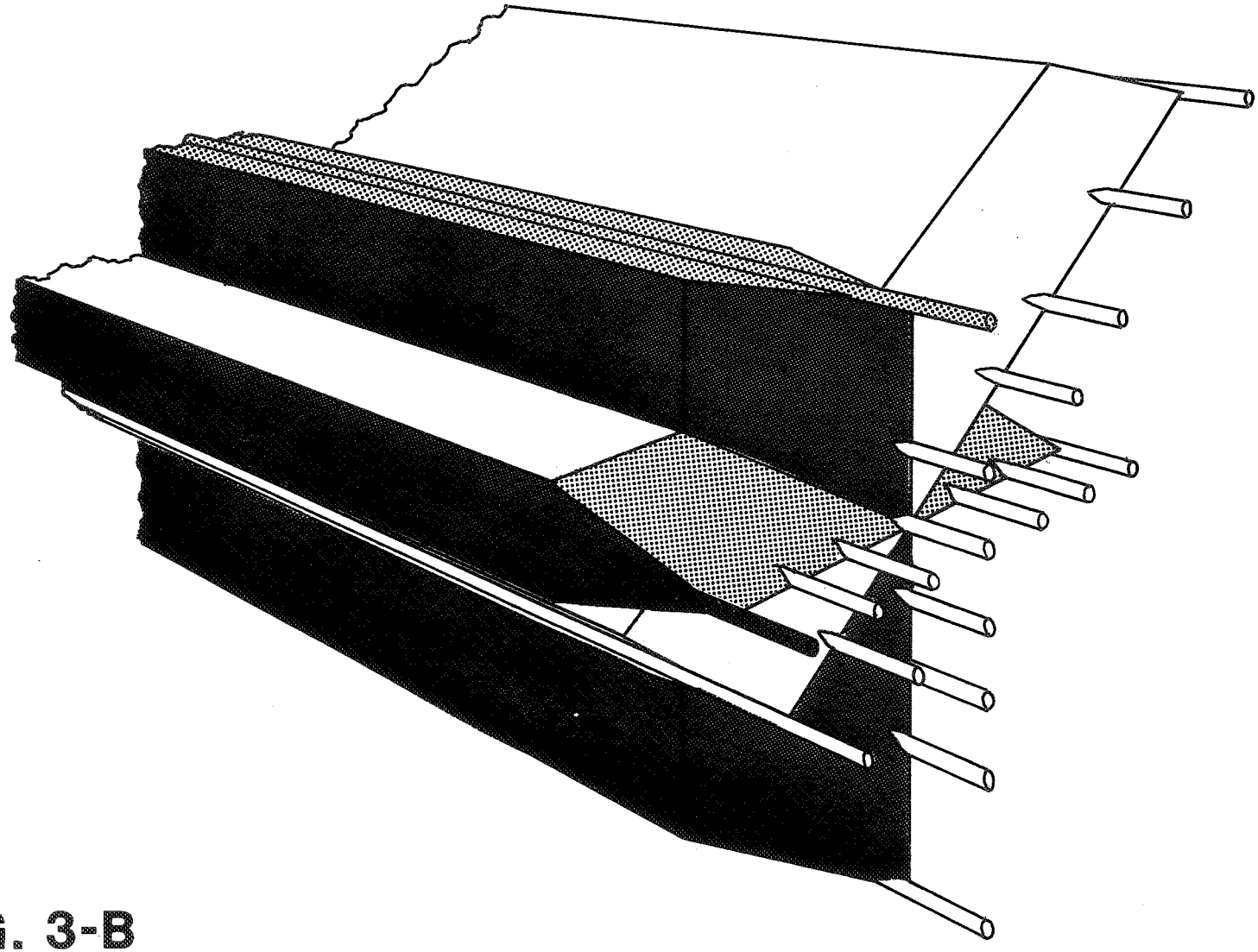

FIG. 3-B
SCHEMATIC DRAWING OF THE RAKE

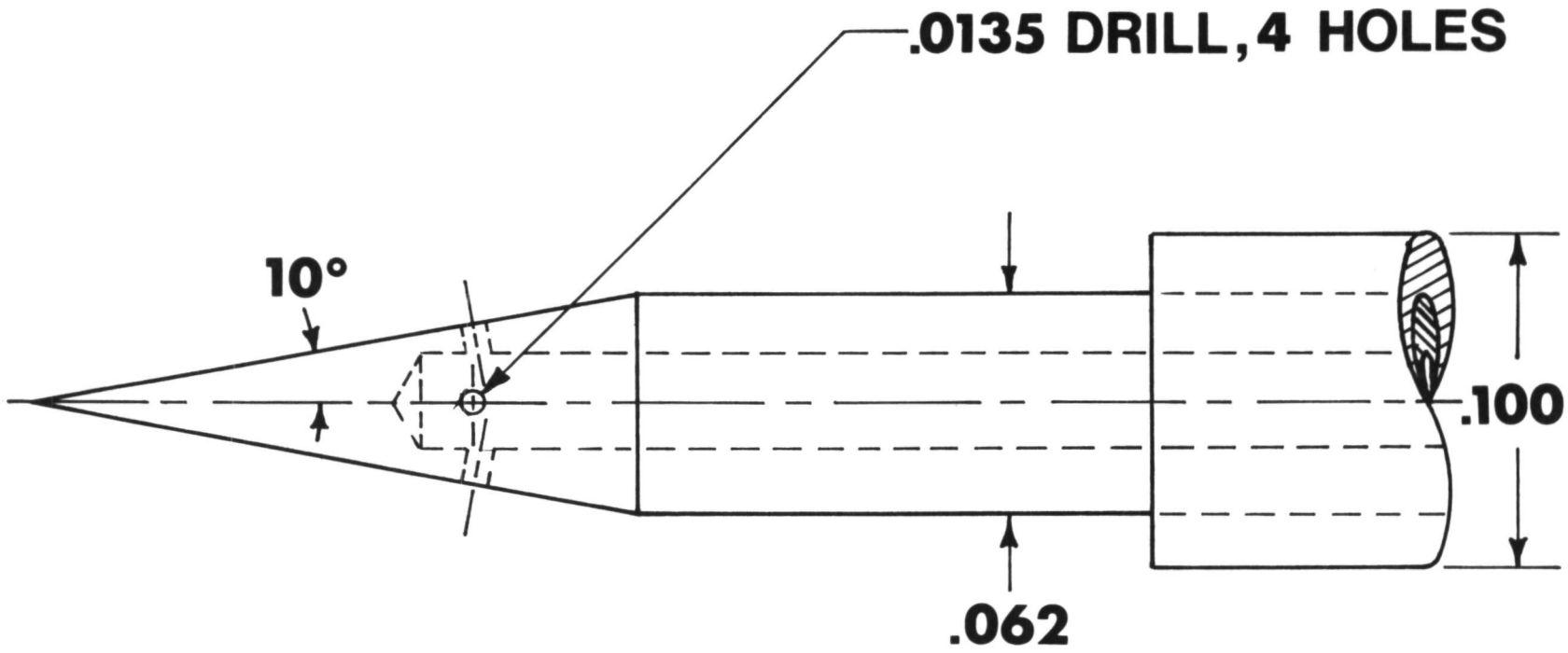

FIG.3-C

THE STATIC PROBE

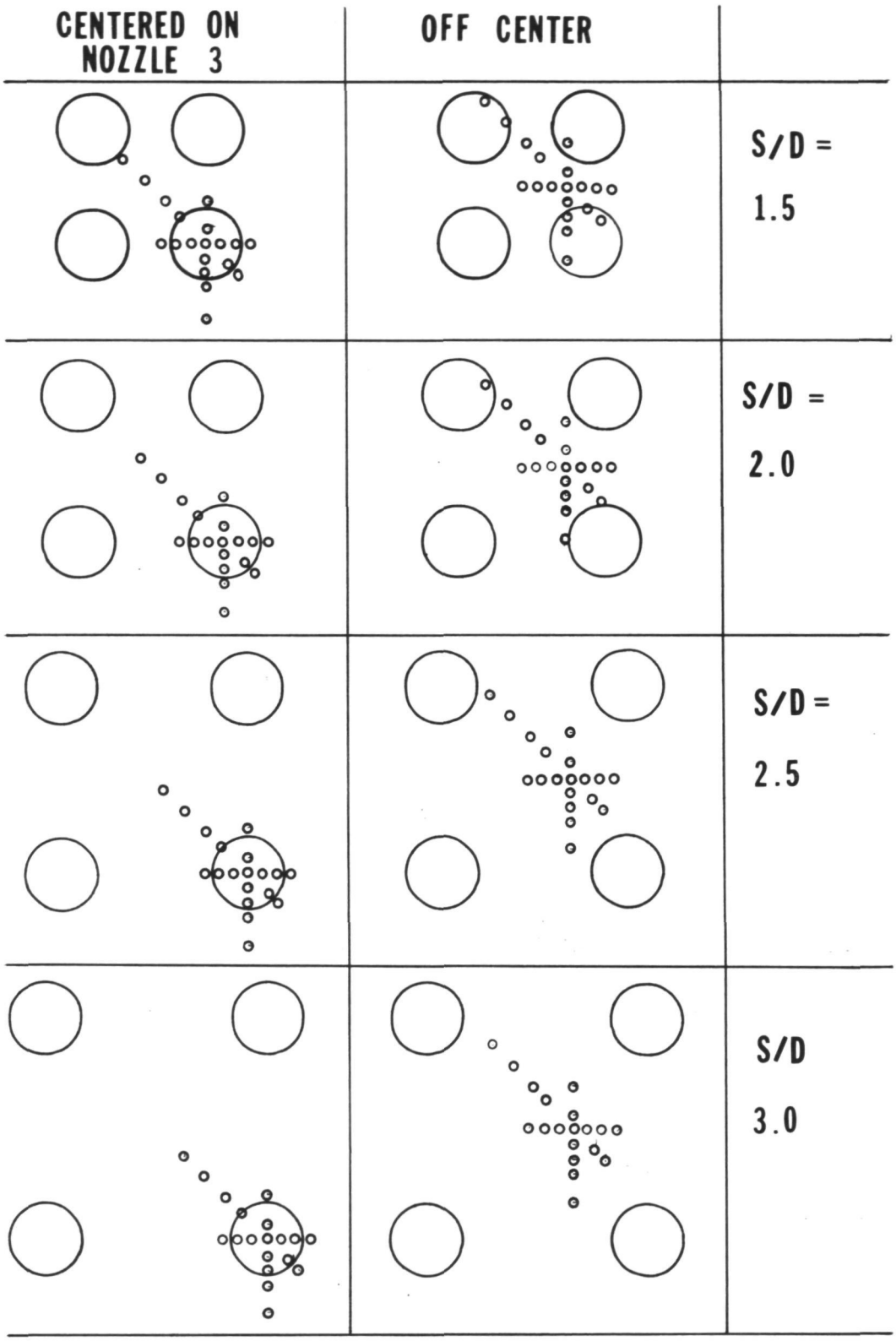

FIG. 4 PROBES' LOCATIONS IN RELATION TO MODEL AT VARIOUS S/D's (FOR MACH NO. MEASUREMENTS ONLY)

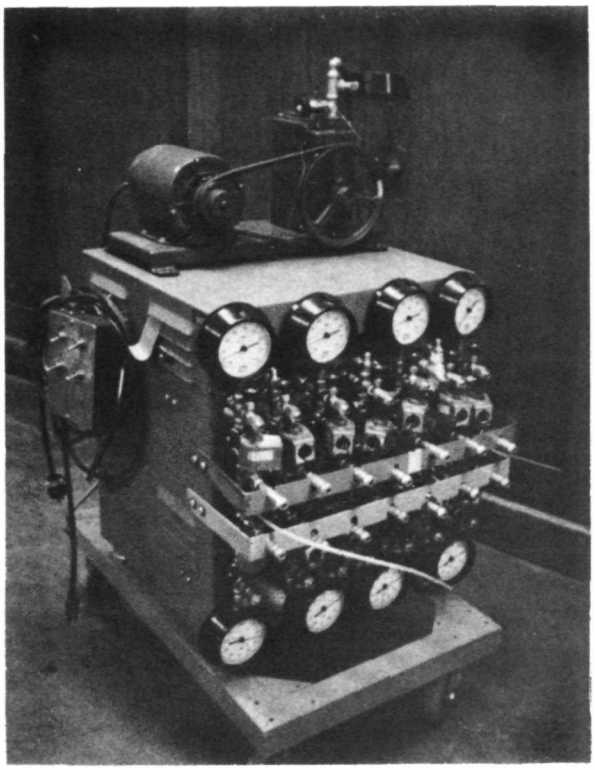

FIG.5

PHOTOGRAPH OF GAS SAMPLE COLLECTION CART

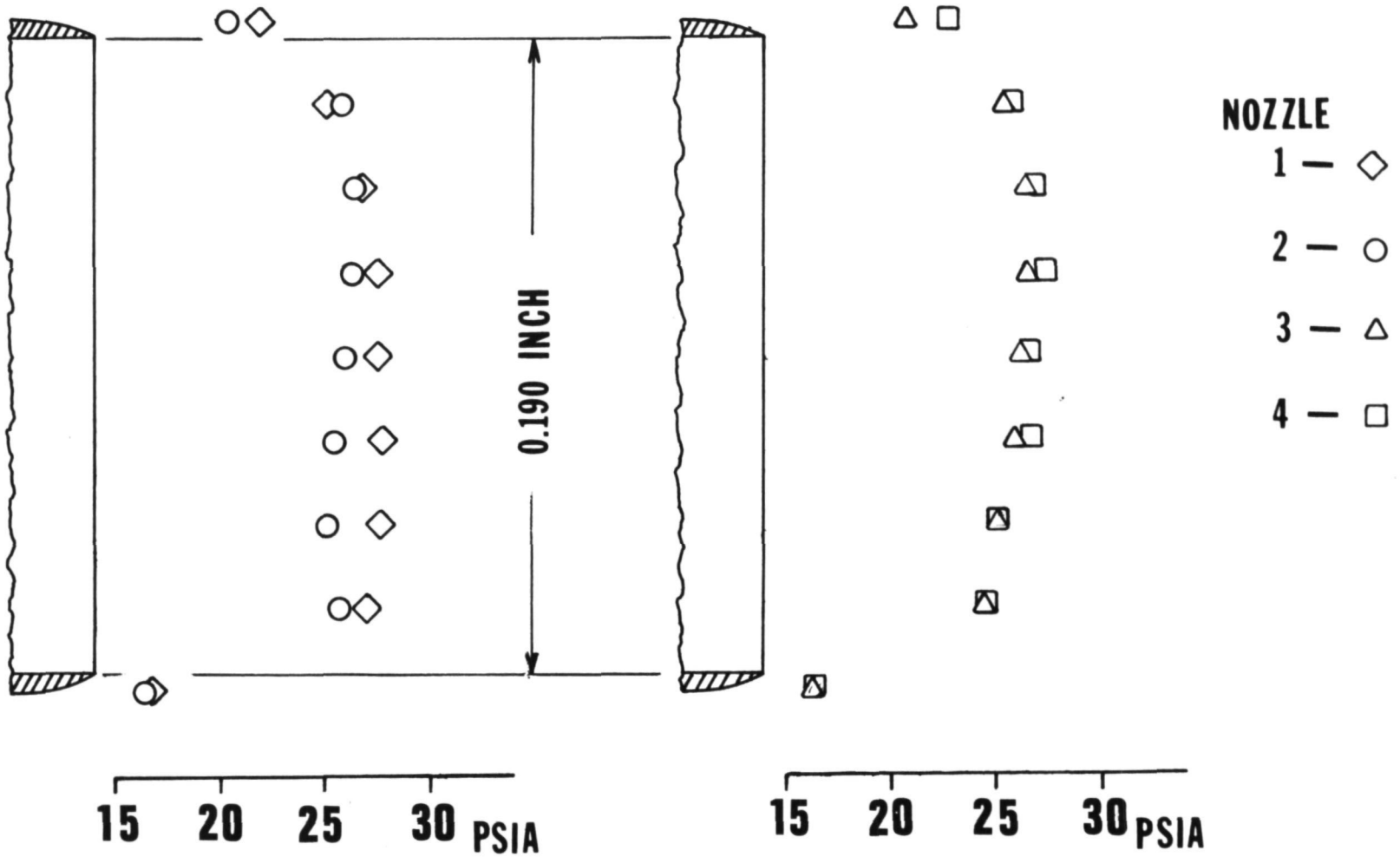

FIG. 6 PITOT PRESSURE DISTRIBUTIONS ACROSS INDIVIDUAL NOZZLES WITH HELIUM INJECTION, NO AIR FLOW

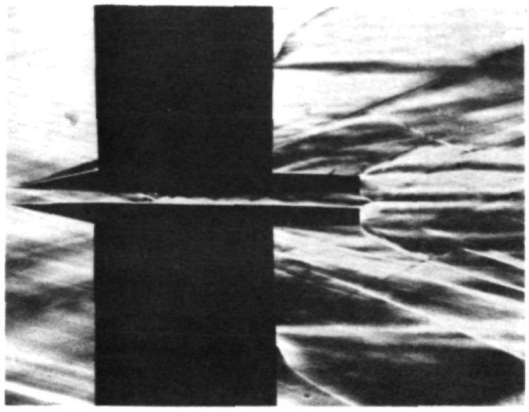

S/D=1.5

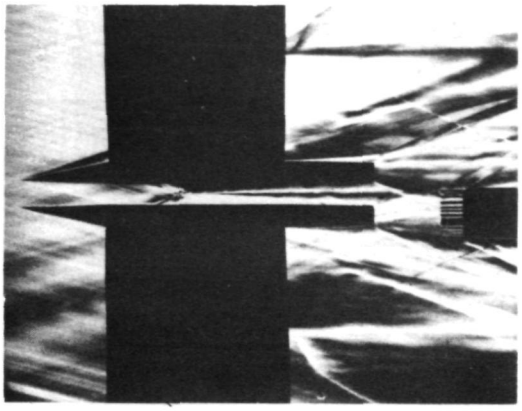

S/D=2.0

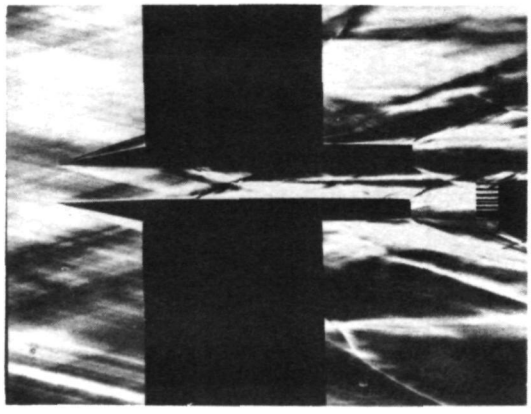

S/D=2.5

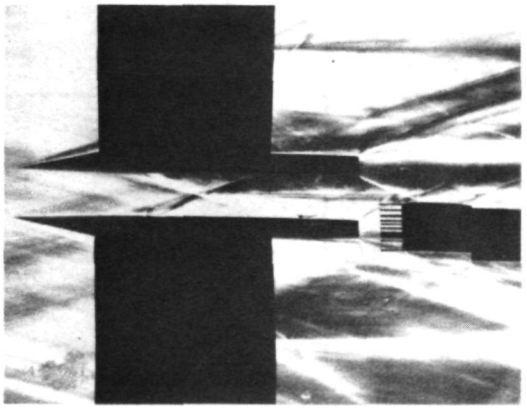

S/D=3.0

FIG. 7

SCHLIEREN PHOTOGRAPHS OF FLOW FIELD OVER THE MODEL FOR VARIOUS S/D's

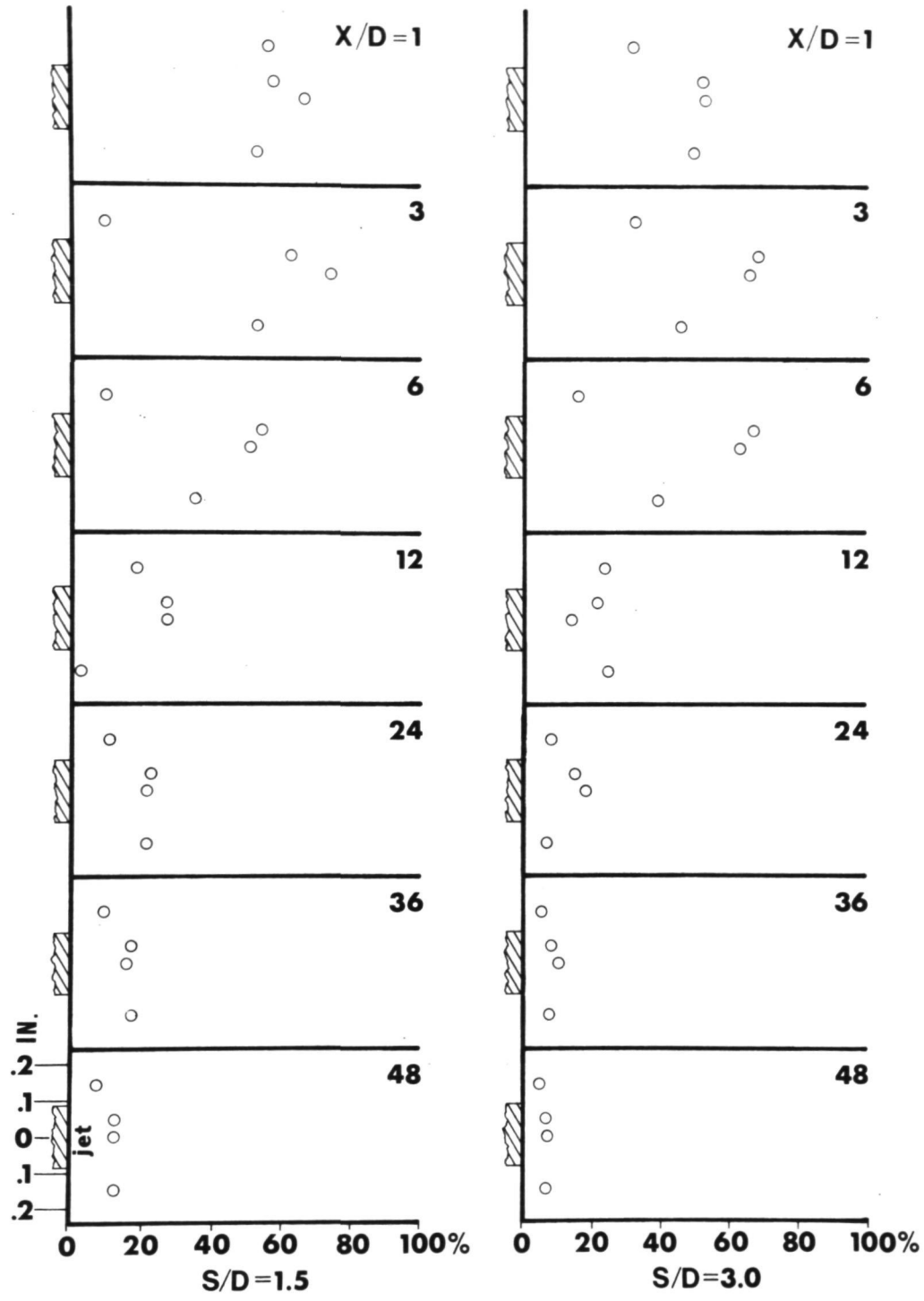

FIG. 8

He CONCENTRATION (MASS FRACTION,%, He)
VERTICAL PROFILES

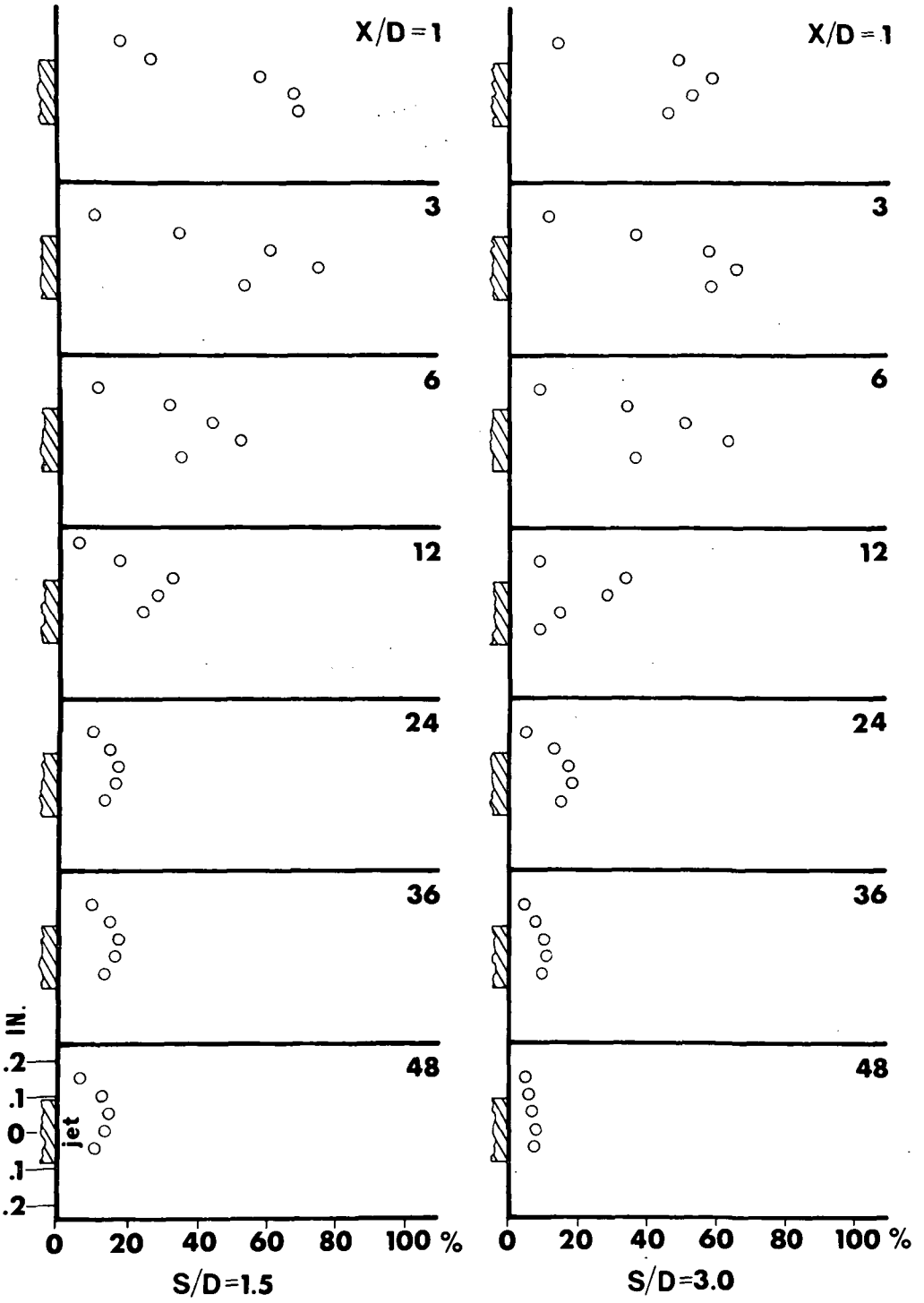

FIG. 9

He CONCENTRATION (MASS FRACTION, %, He) HORIZONTAL PROFILES

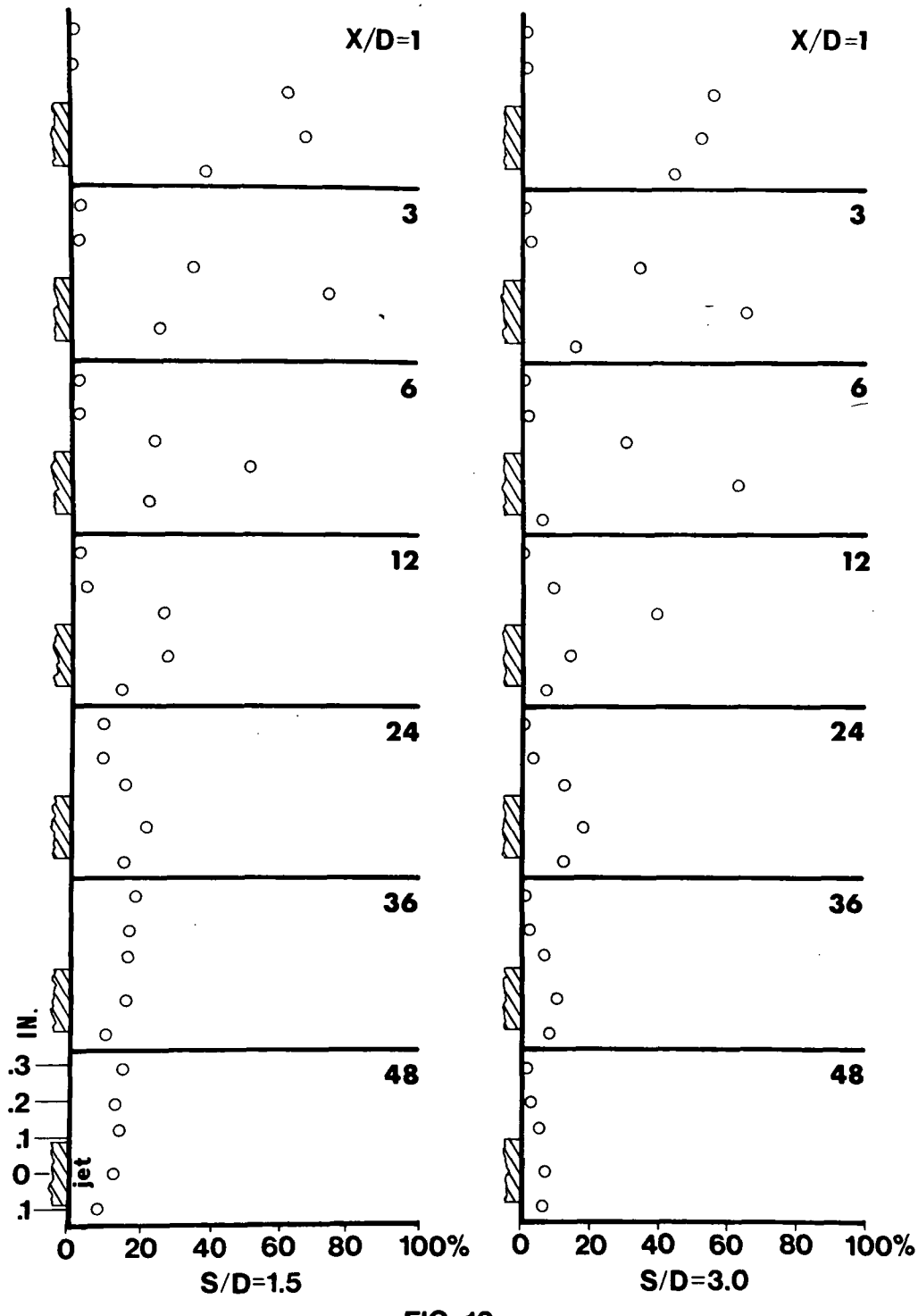

FIG. 10

He CONCENTRATION (MASS FRACTION,%,He)
DIAGONAL PROFILES

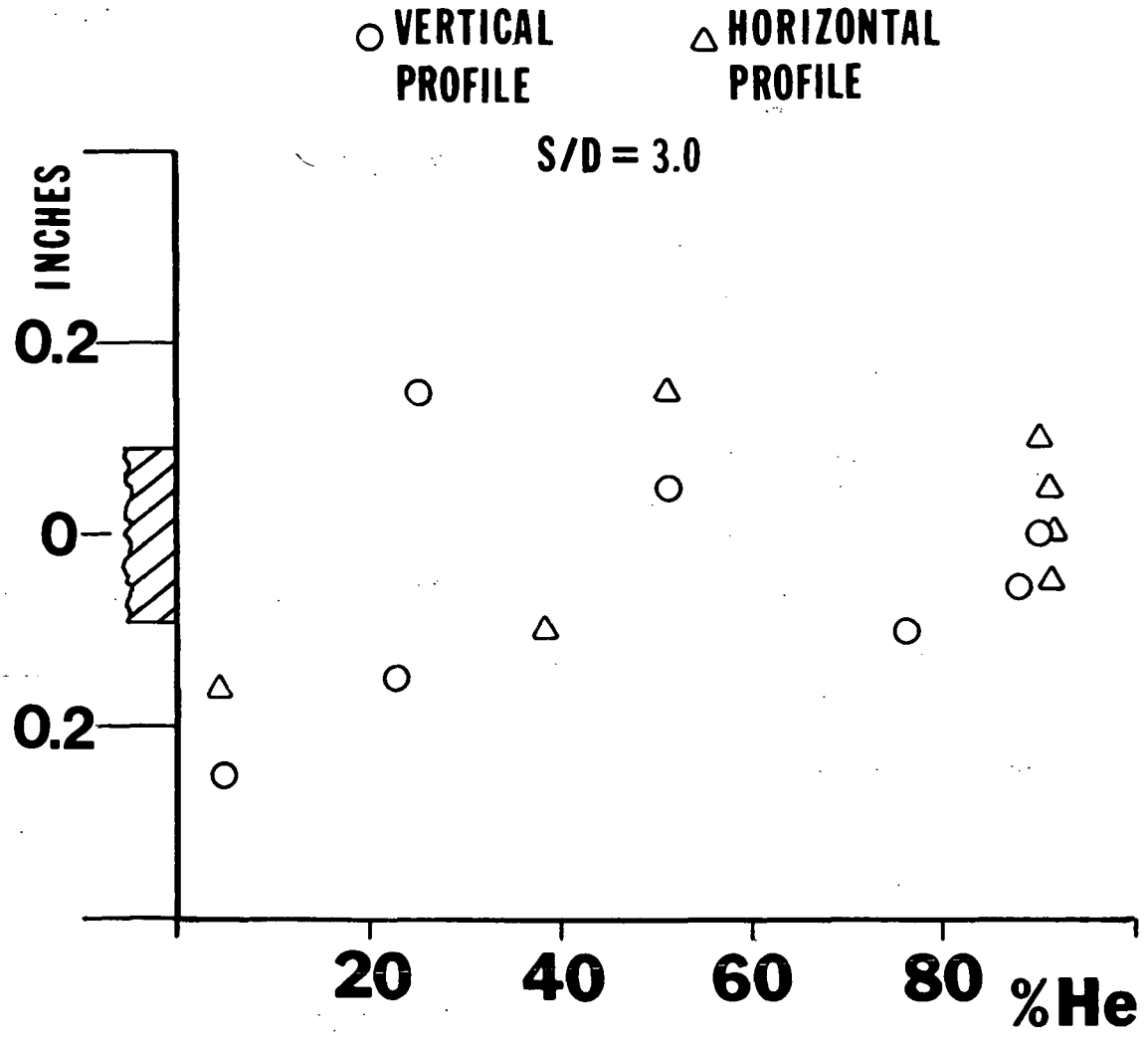

FIG. 11

He CONCENTRATION (MASS FRACTION, %, He) AT X/D=0.1

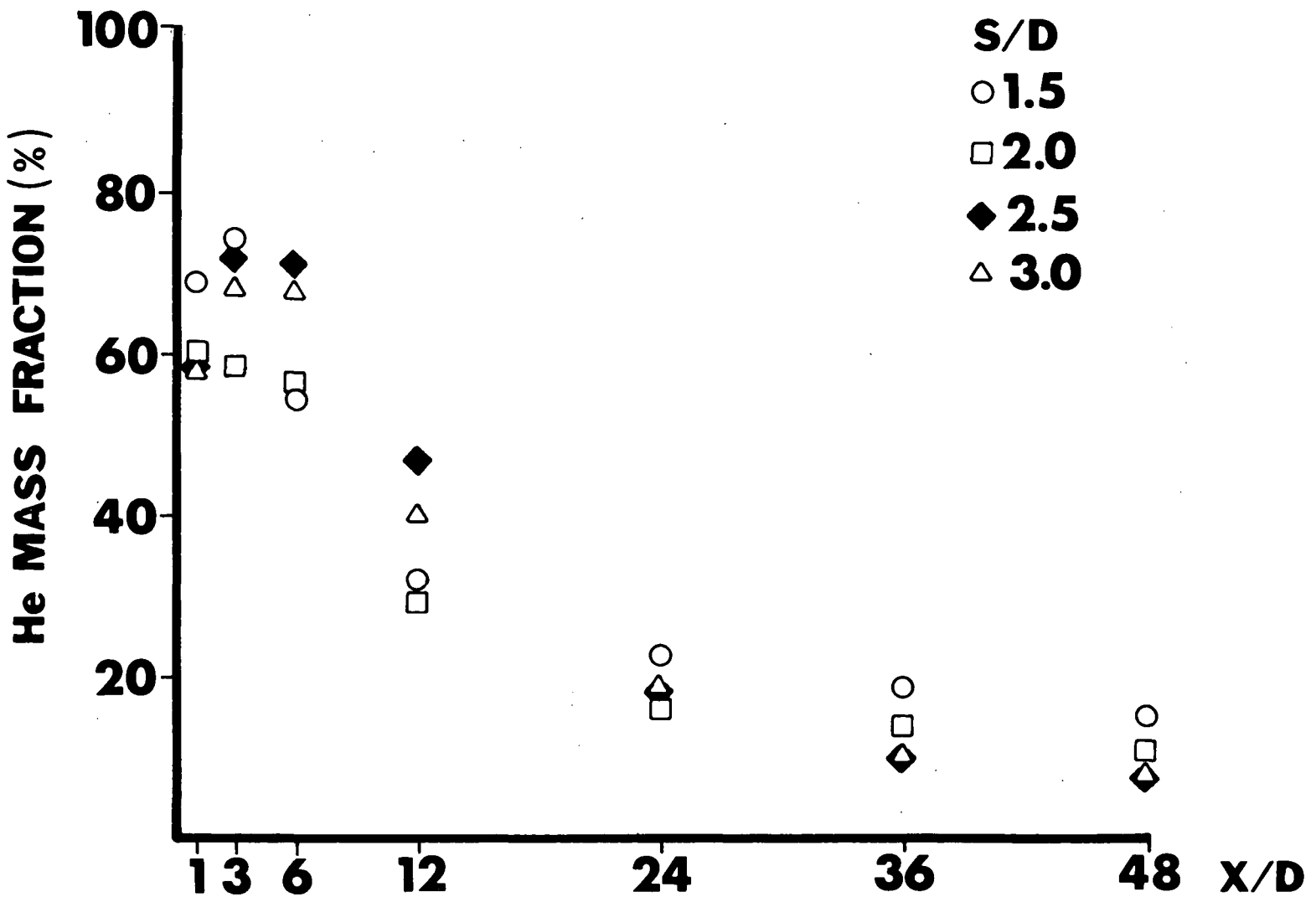

FIG. 12 MAXIMUM He CONCENTRATION AS A FUNCTION OF DISTANCE FROM INJECTOR FOR VARIOUS S/D's

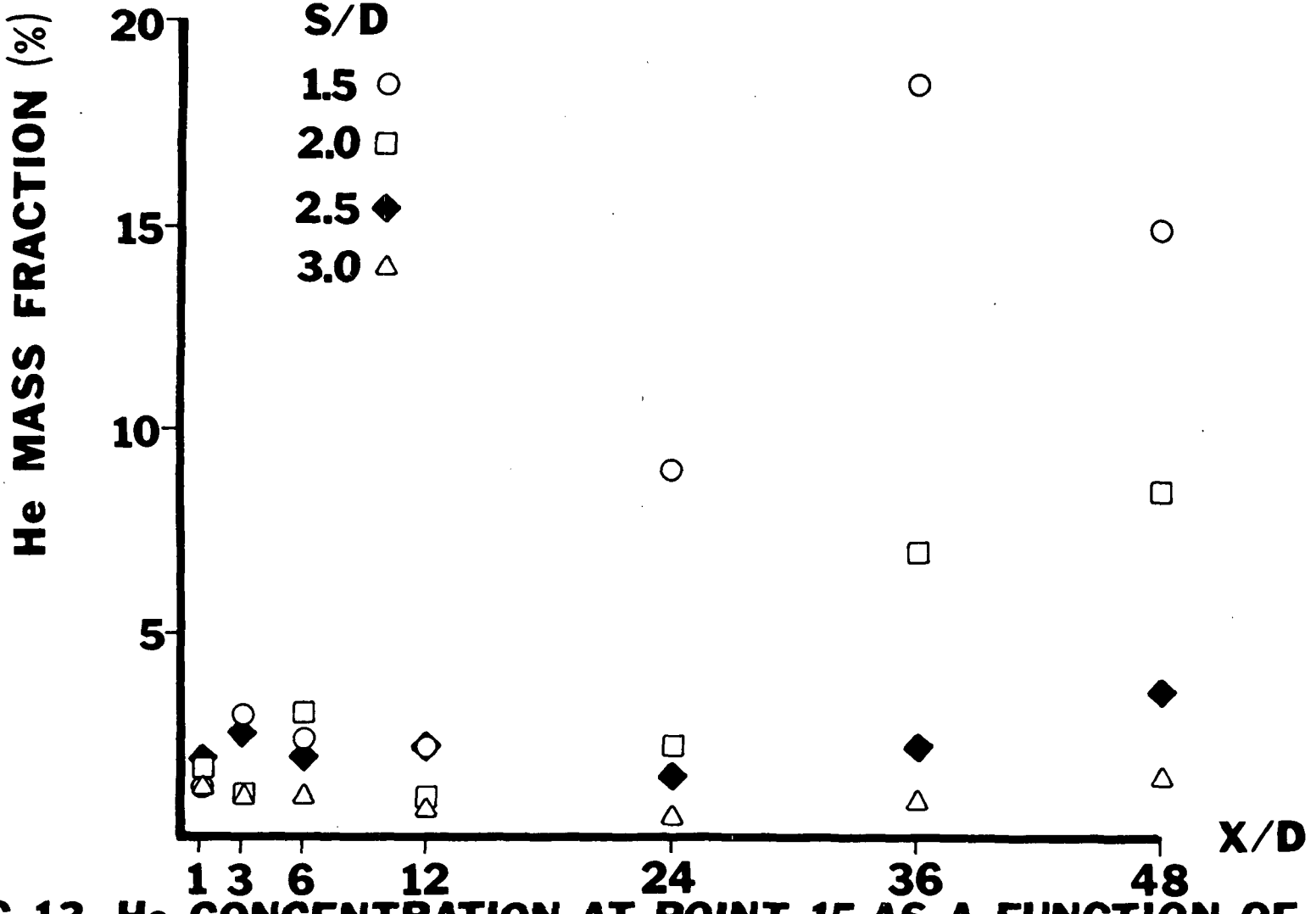

FIG. 13 He CONCENTRATION AT POINT 15 AS A FUNCTION OF DISTANCE FROM INJECTOR FOR VARIOUS S/D's

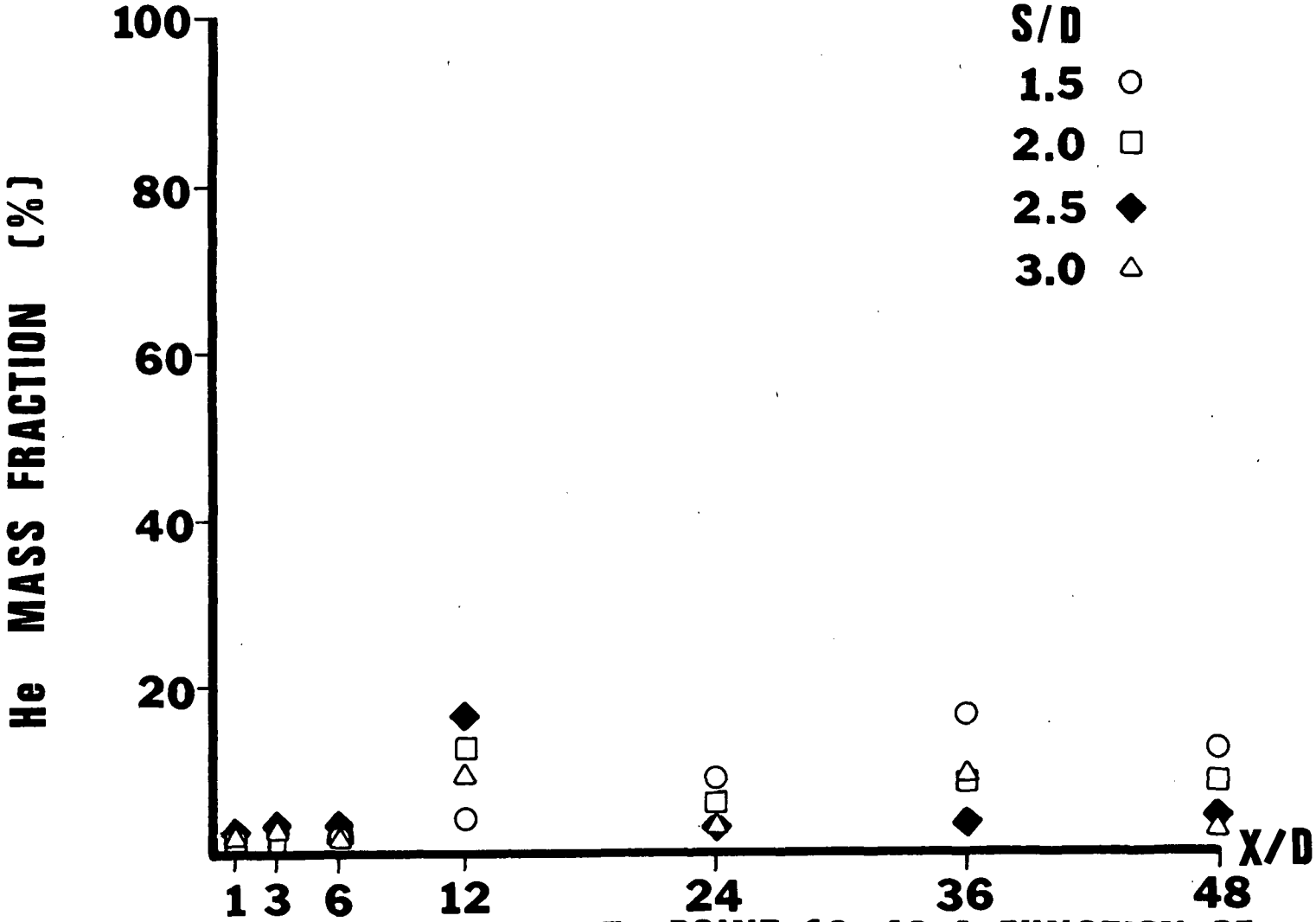

FIG. 14 He CONCENTRATION AT POINT 16 AS A FUNCTION OF DISTANCE FROM INJECTOR FOR VARIOUS S/D's

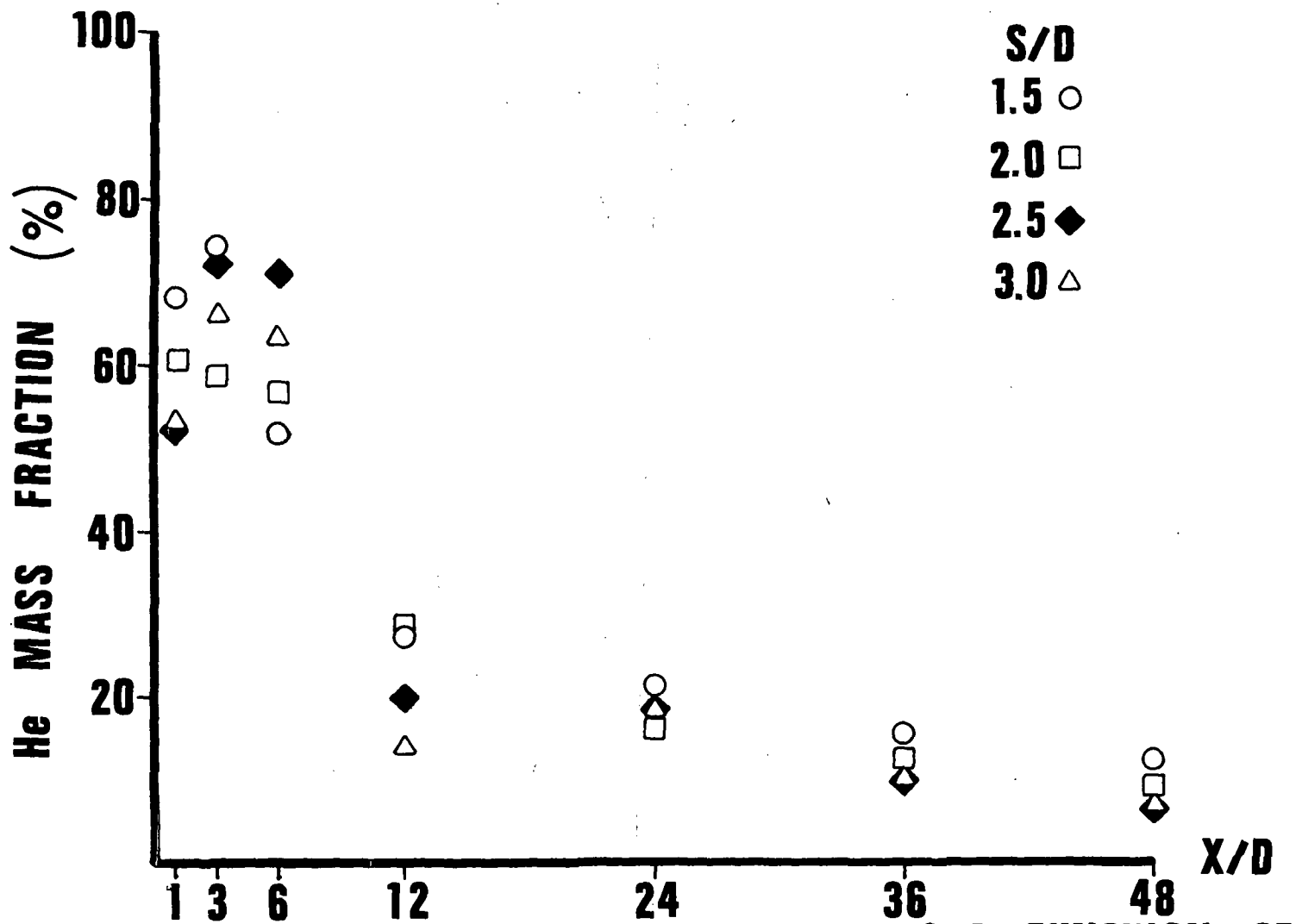

FIG. 15 He CONCENTRATION AT POINT 3 AS A FUNCTION OF DISTANCE FROM INJECTOR FOR VARIOUS S/D's

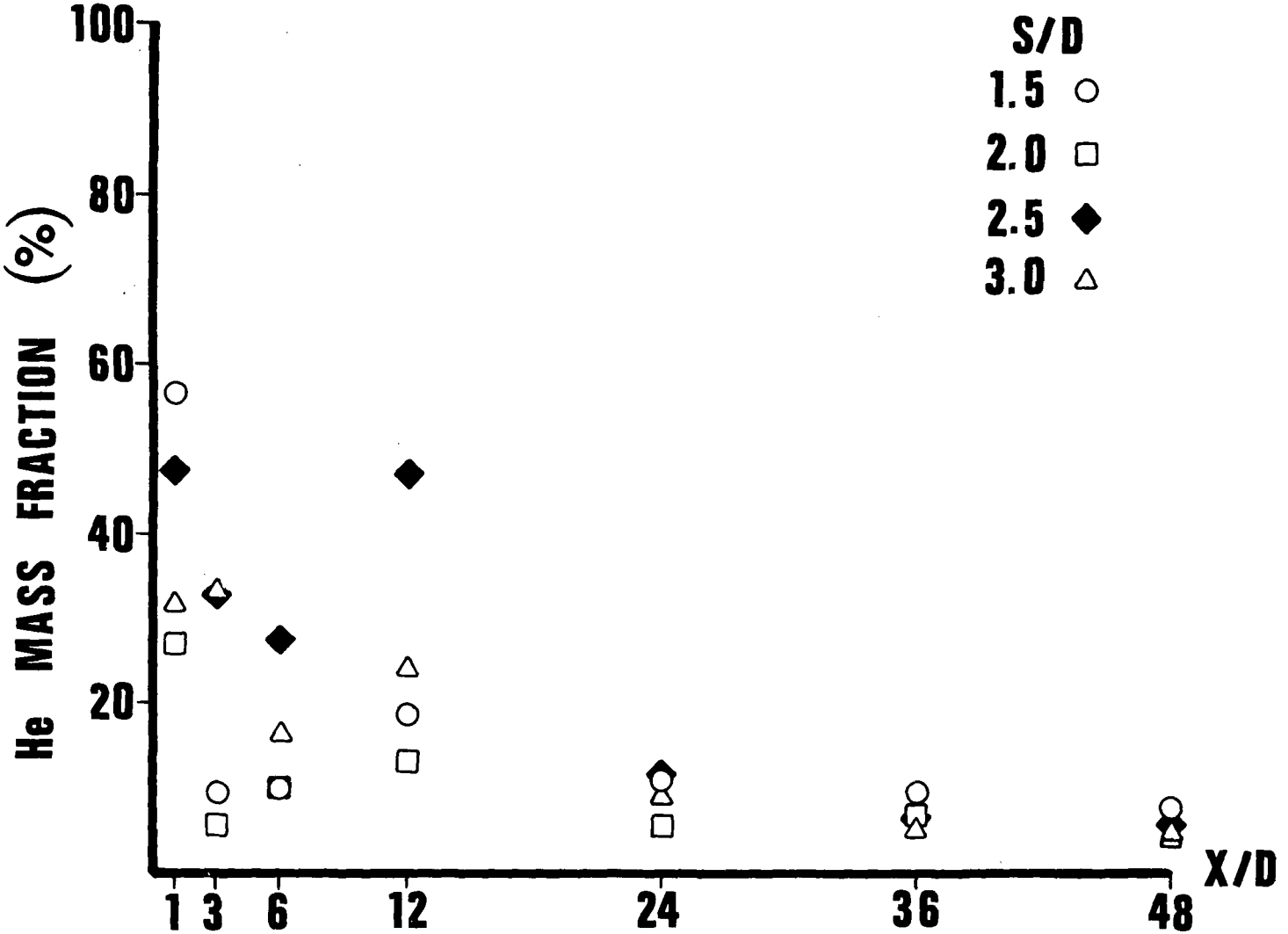

FIG. 16 He CONCENTRATION AT POINT 1 AS A FUNCTION OF DISTANCE FROM INJECTOR FOR VARIOUS S/D's

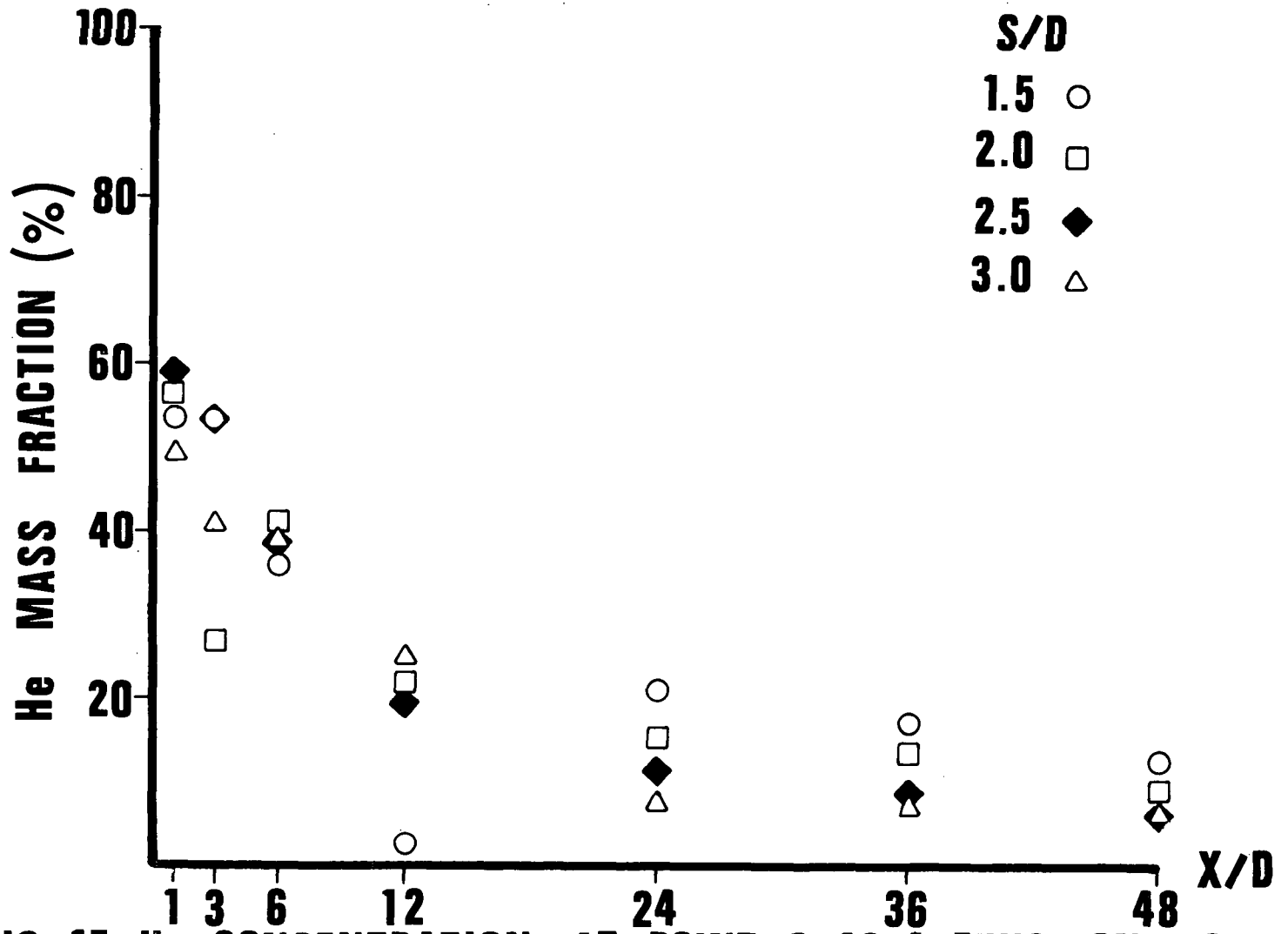

FIG. 17 He CONCENTRATION AT POINT 6 AS A FUNCTION OF DISTANCE FROM INJECTOR FOR VARIOUS S/D's

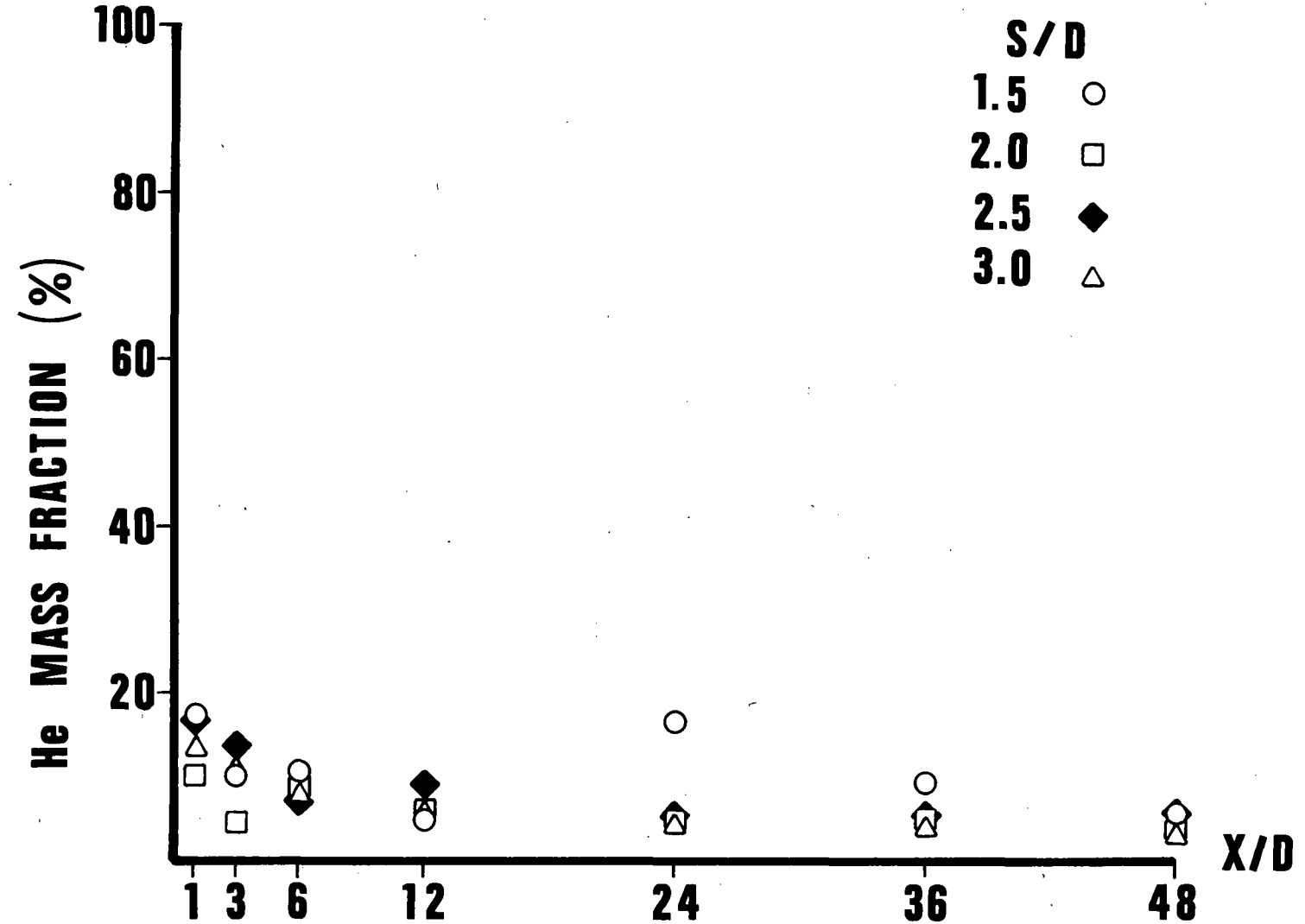

FIG. 18 He CONCENTRATION AT POINT 8 AS A FUNCTION OF DISTANCE FROM INJECTOR FOR VARIOUS S/D's

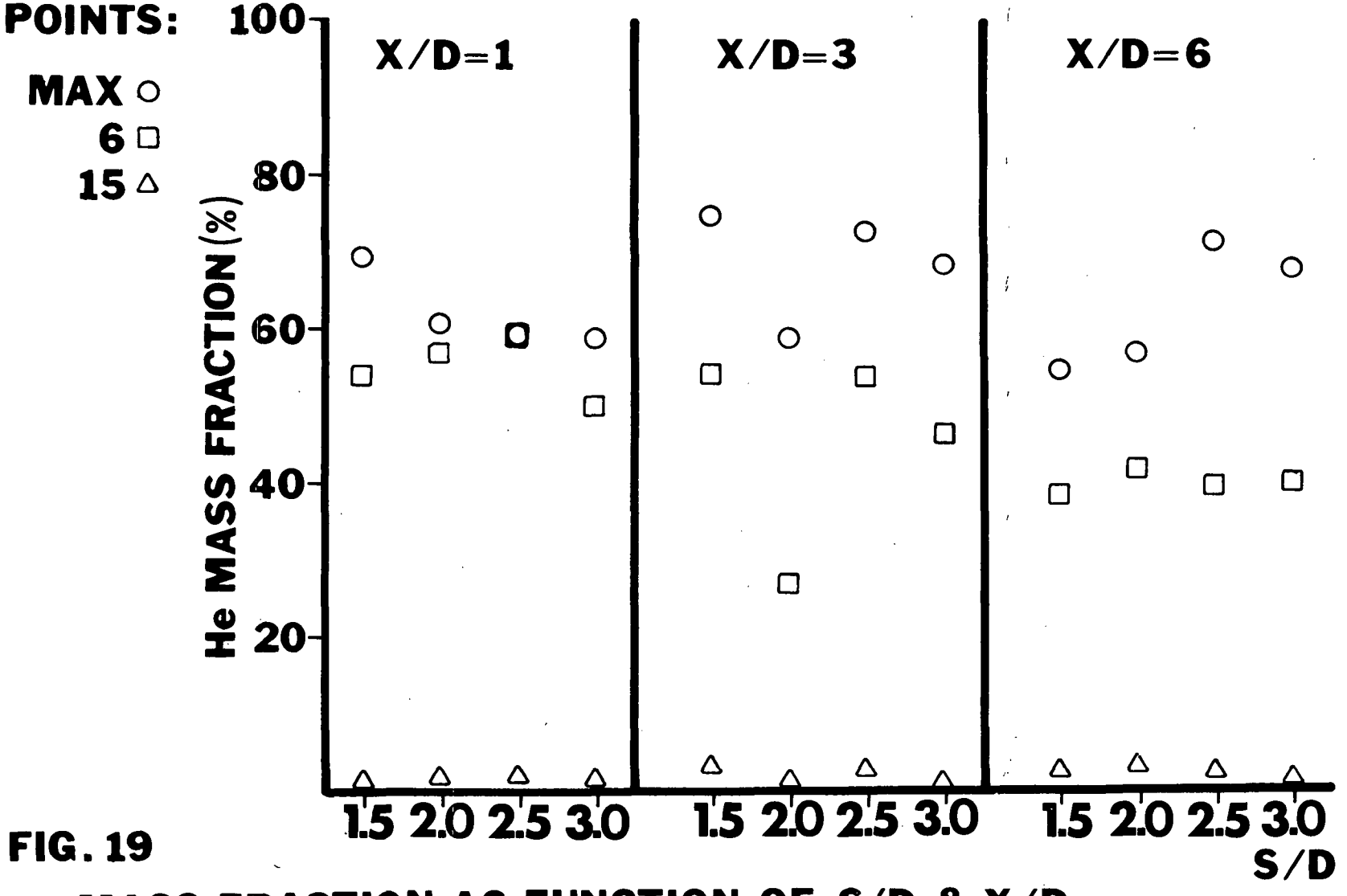

FIG. 19

He MASS FRACTION AS FUNCTION OF S/D & X/D

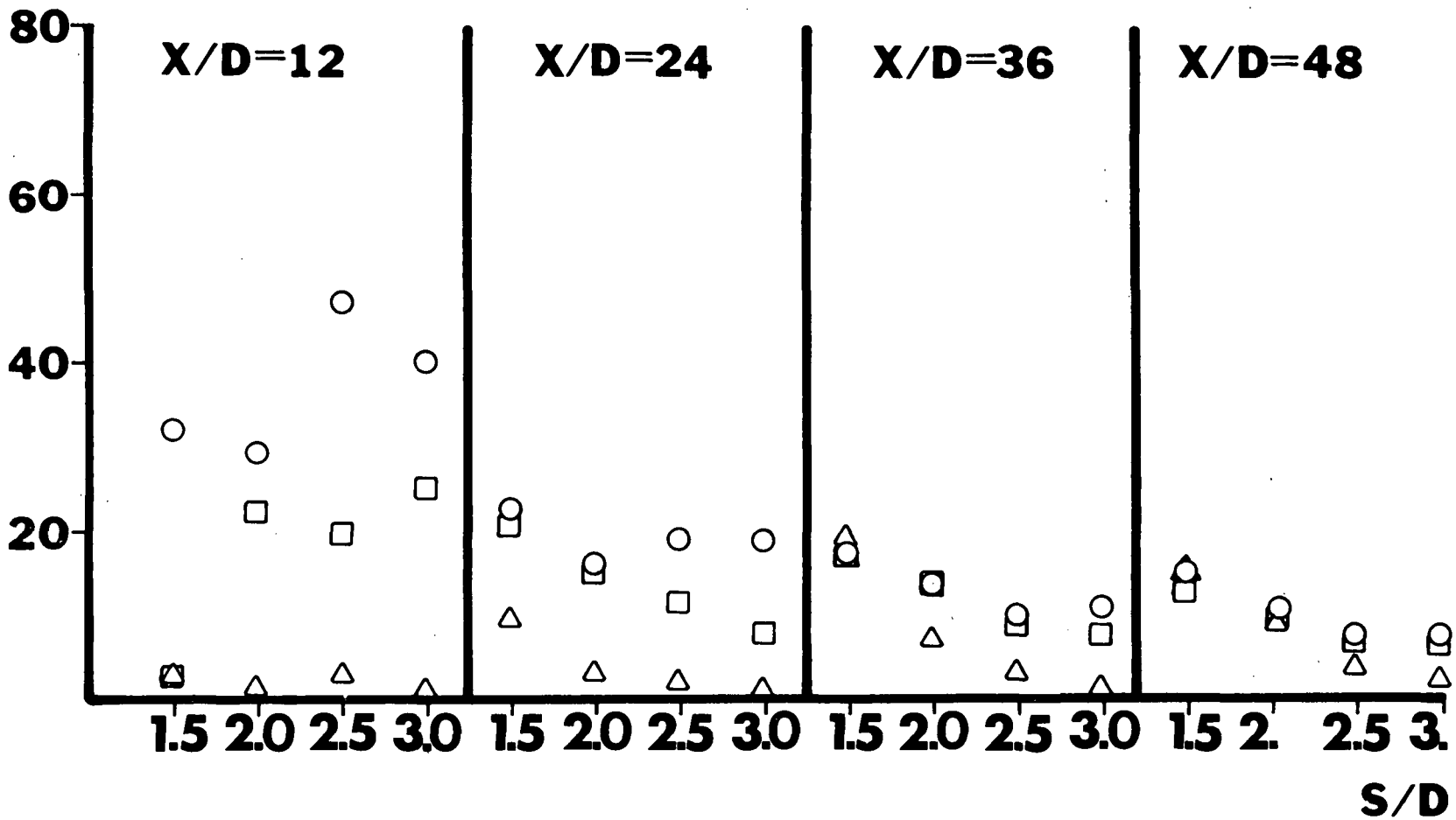
80
60
40
20
X/D=12
X/D=24
X/D=36
X/D=48
1.5 2.0 2.5 3.0 1.5 2.0 2.5 3.0 1.5 2.0 2.5 3.0 1.5 2. 2.5 3.
S/D

FIG. 19 (CONT'D)

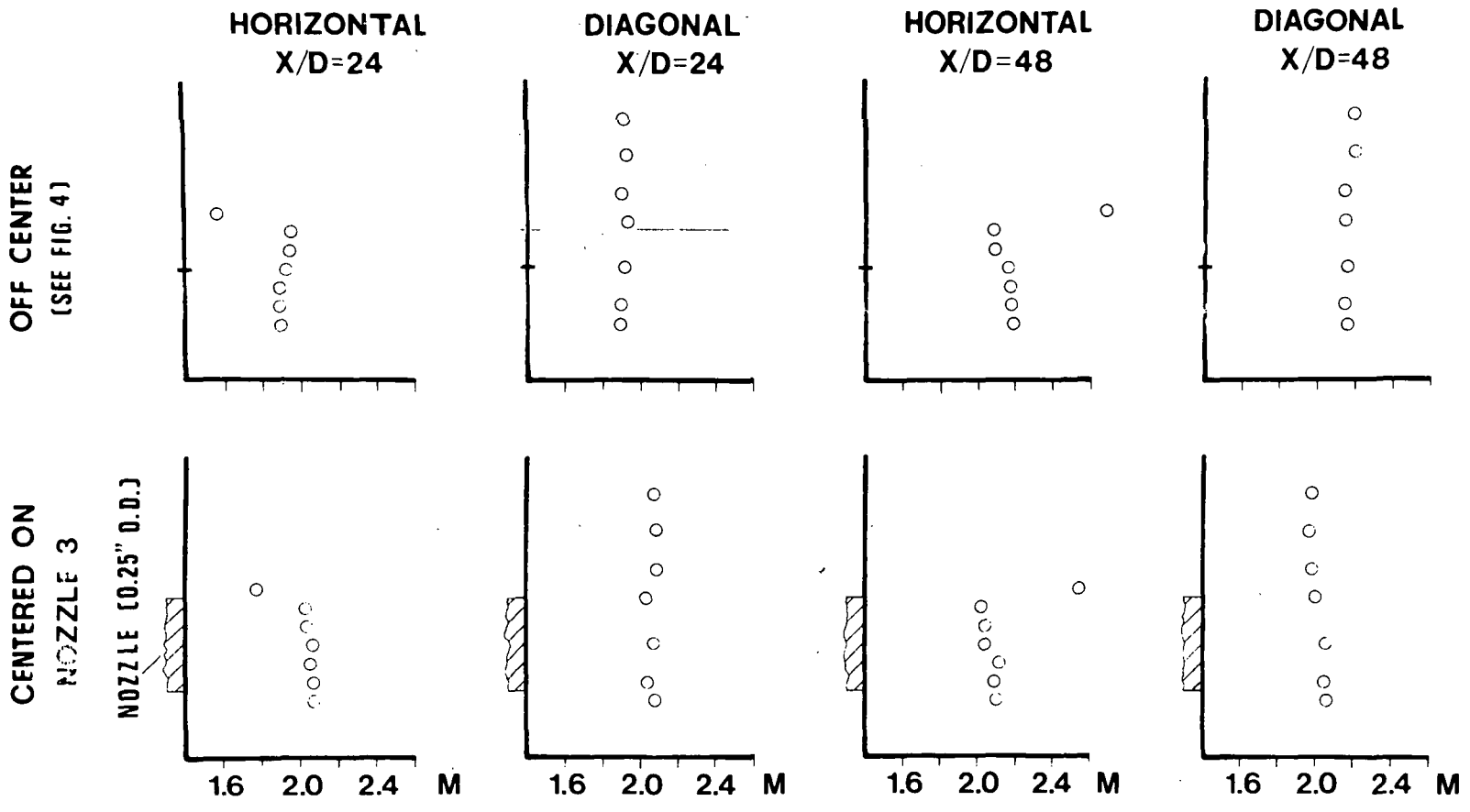

FIG. 20-A

MACH No. DISTRIBUTION ACROSS MODEL AT S/D=1.5

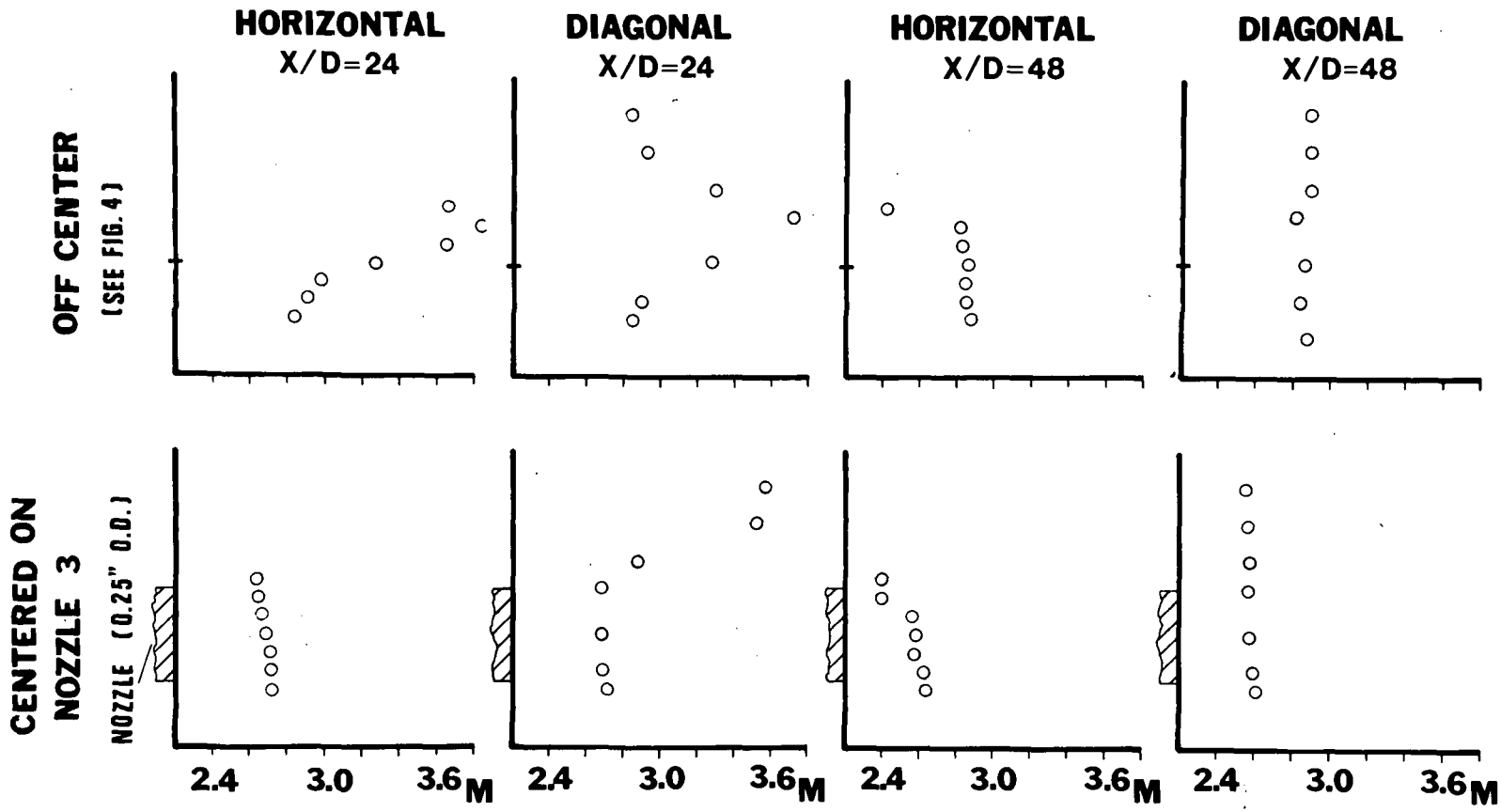

FIG. 20-B

MACH No. DISTRIBUTION ACROSS MODEL AT S/D=2.0

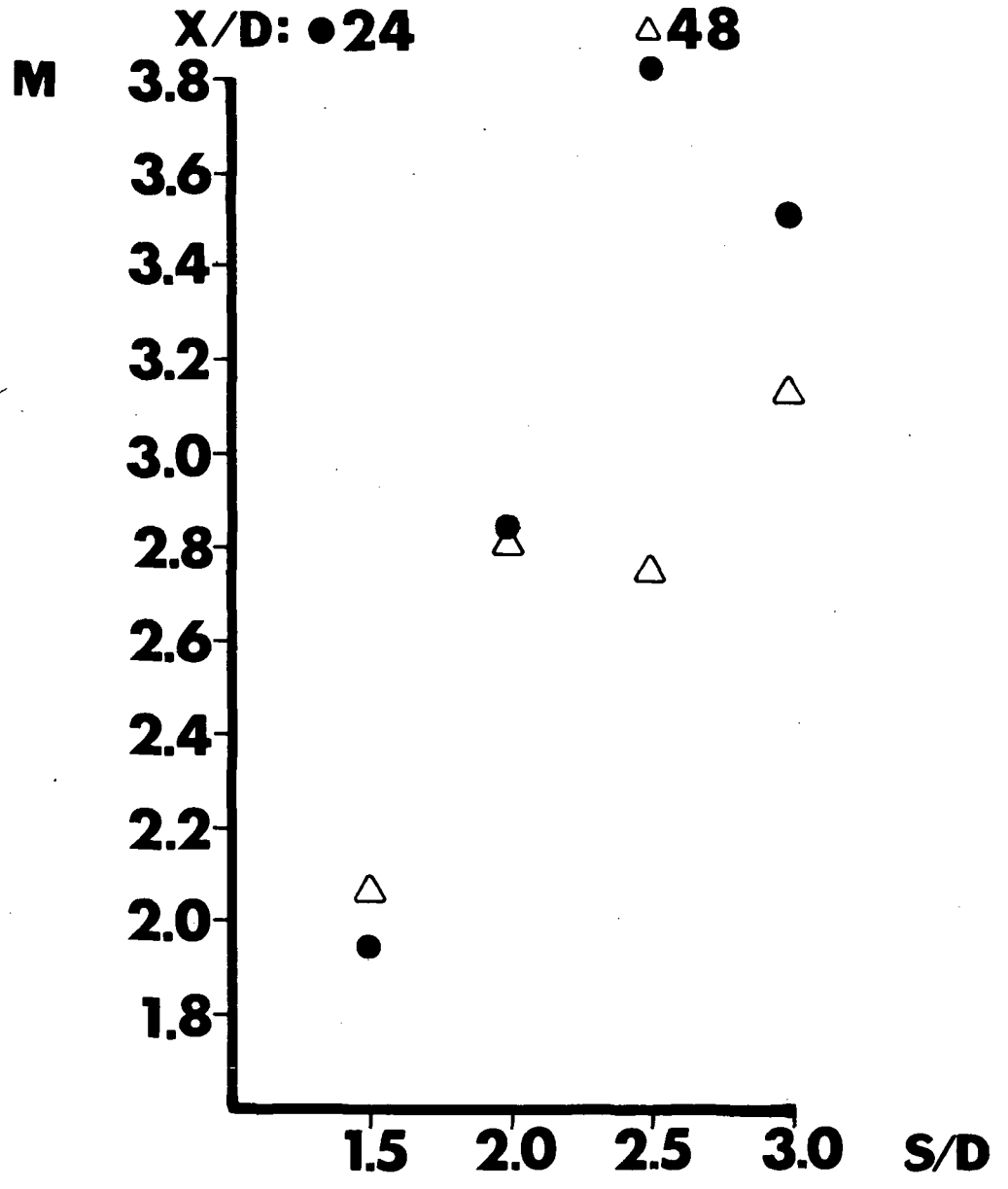

FIG. 21

MACH No. AS FUNCTION OF S/D FOR PT. 9

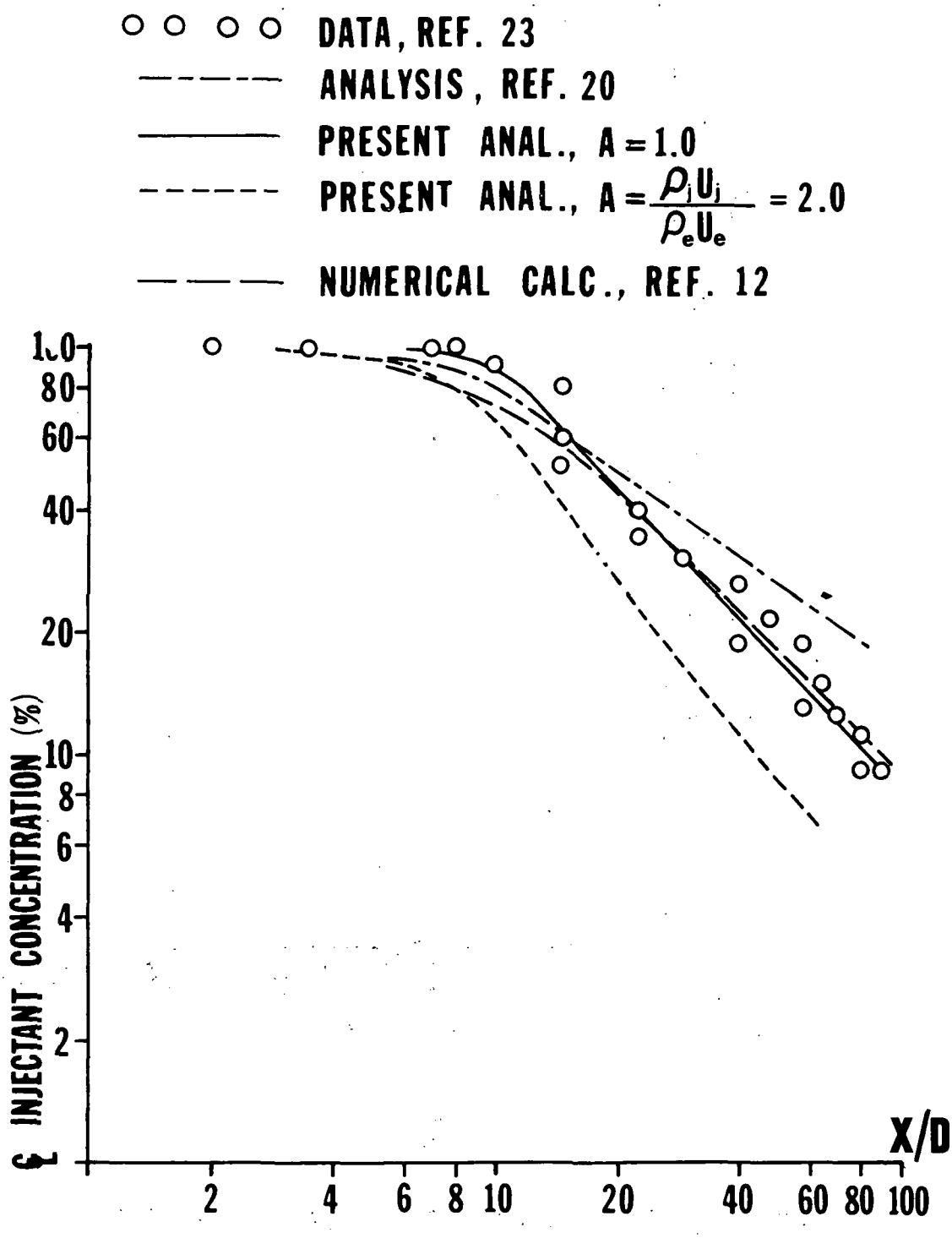

FIG. 22 COMPARISON OF PRESENT THEORETICAL CALCULATION WITH EXPERIMENTAL DATA FROM REF. 23

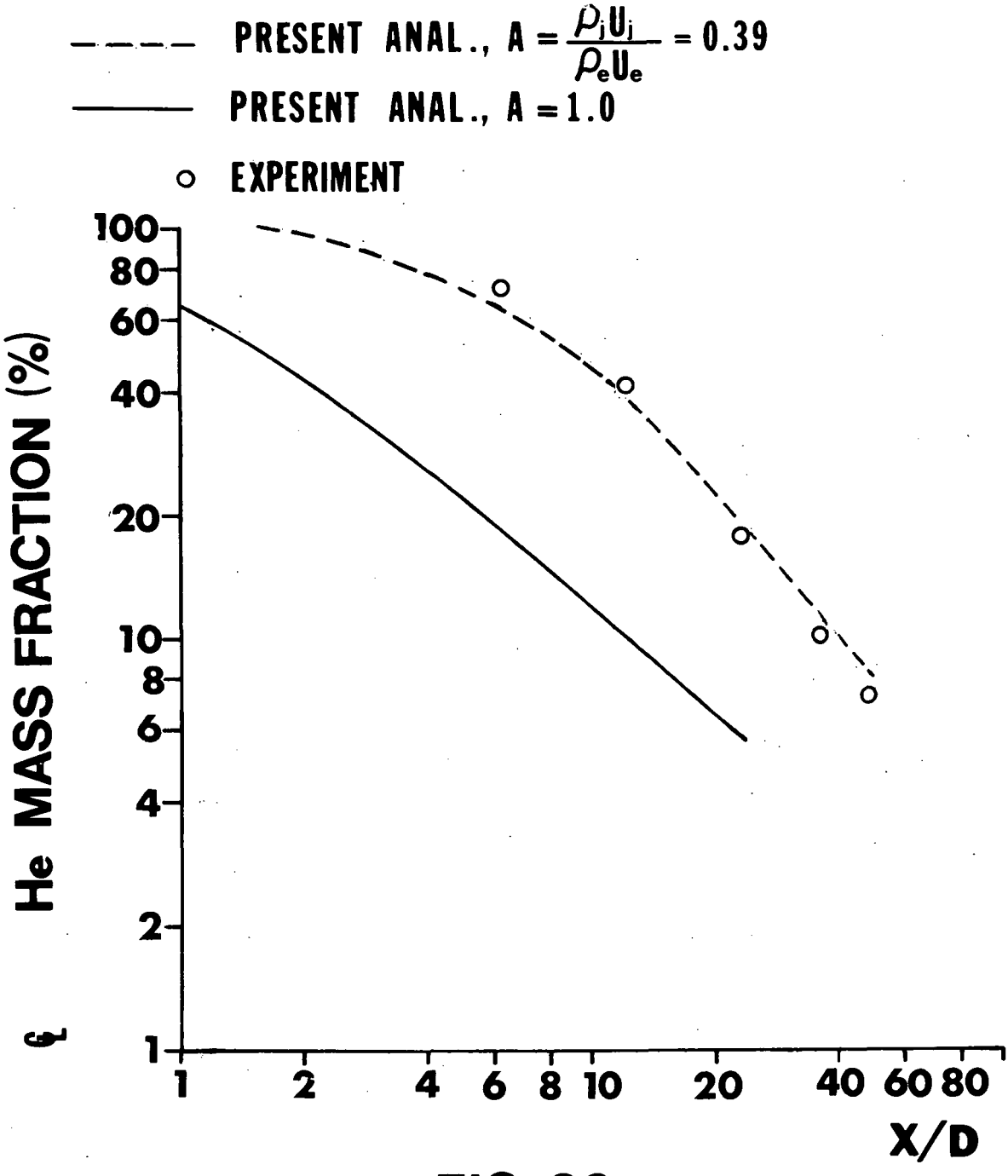

FIG. 23

COMPARISON OF PRESENT THEORETICAL CALCULATIONS WITH PRESENT EXPERIMENTAL RESULTS

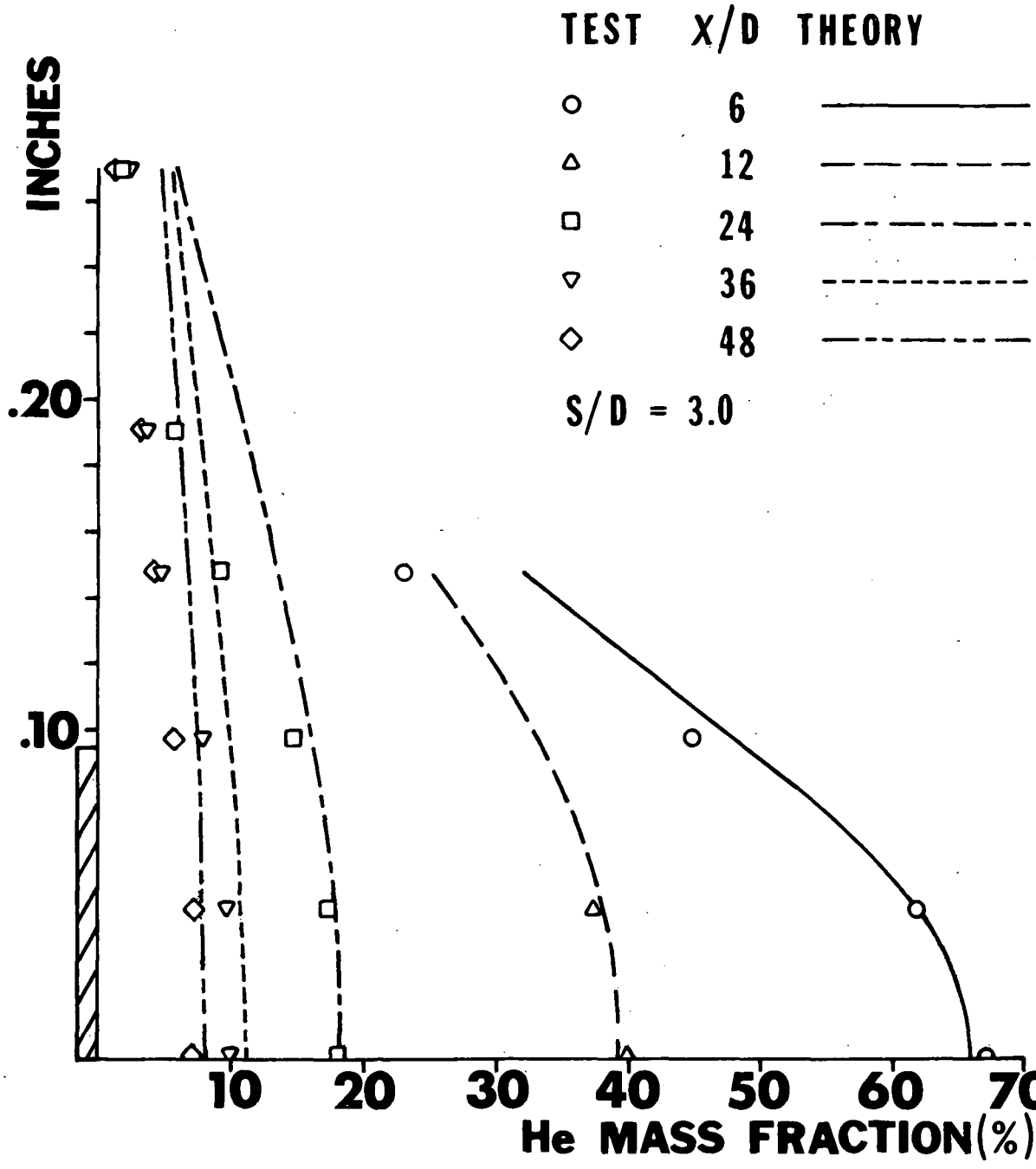

FIG. 24 CONCENTRATION PROFILES VS. RADIAL DISTANCE FROM NOZZLE CENTER LINE FOR VARIOUS X/D's (COMPARISON BETWEEN THEORY AND EXPERIMENT)

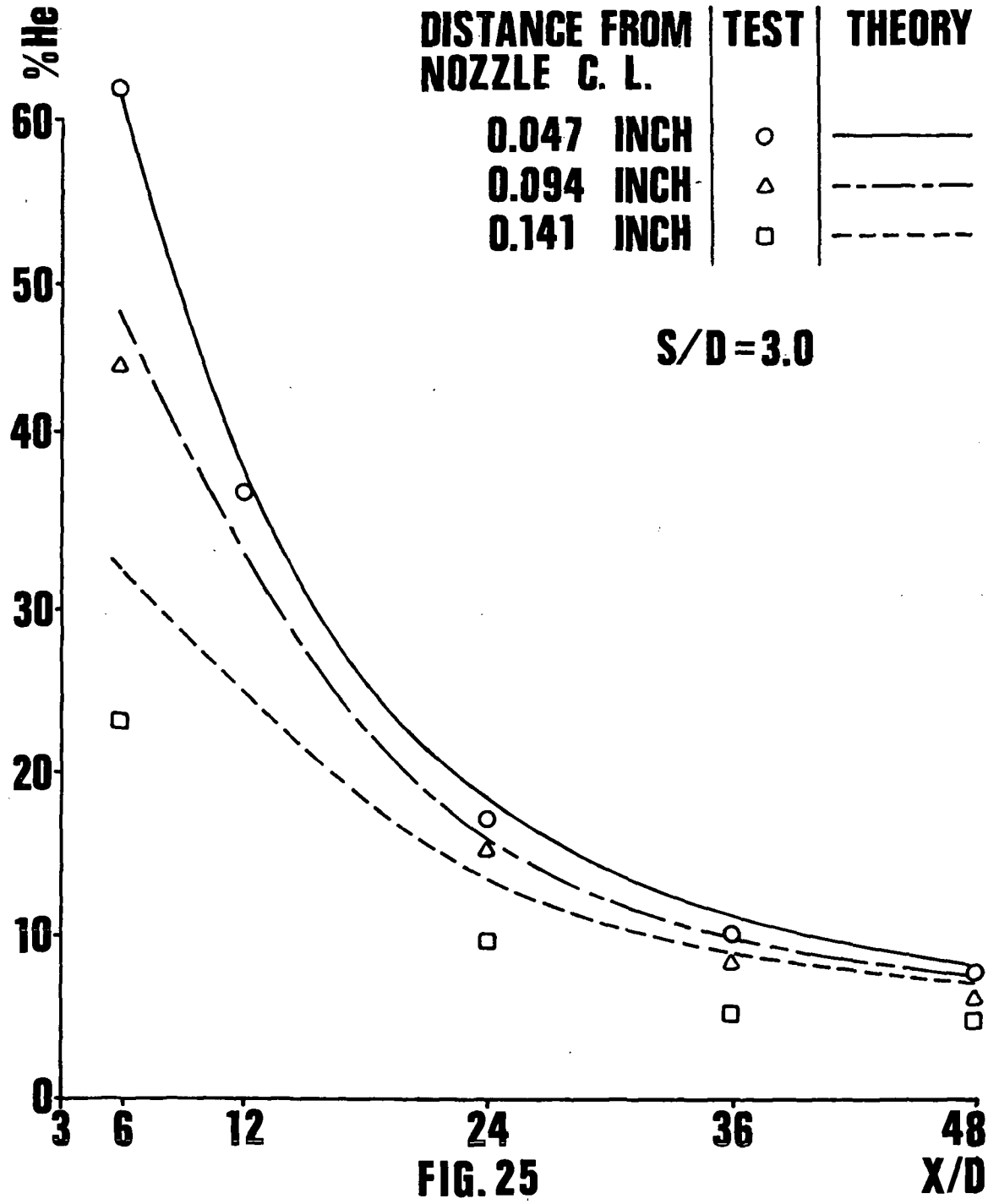

FIG. 25

He CONCENTRATION VS. X/D FOR VARIOUS RADIAL DISTANCES; COMPARISON BETWEEN THEORY AND EXPERIMENT

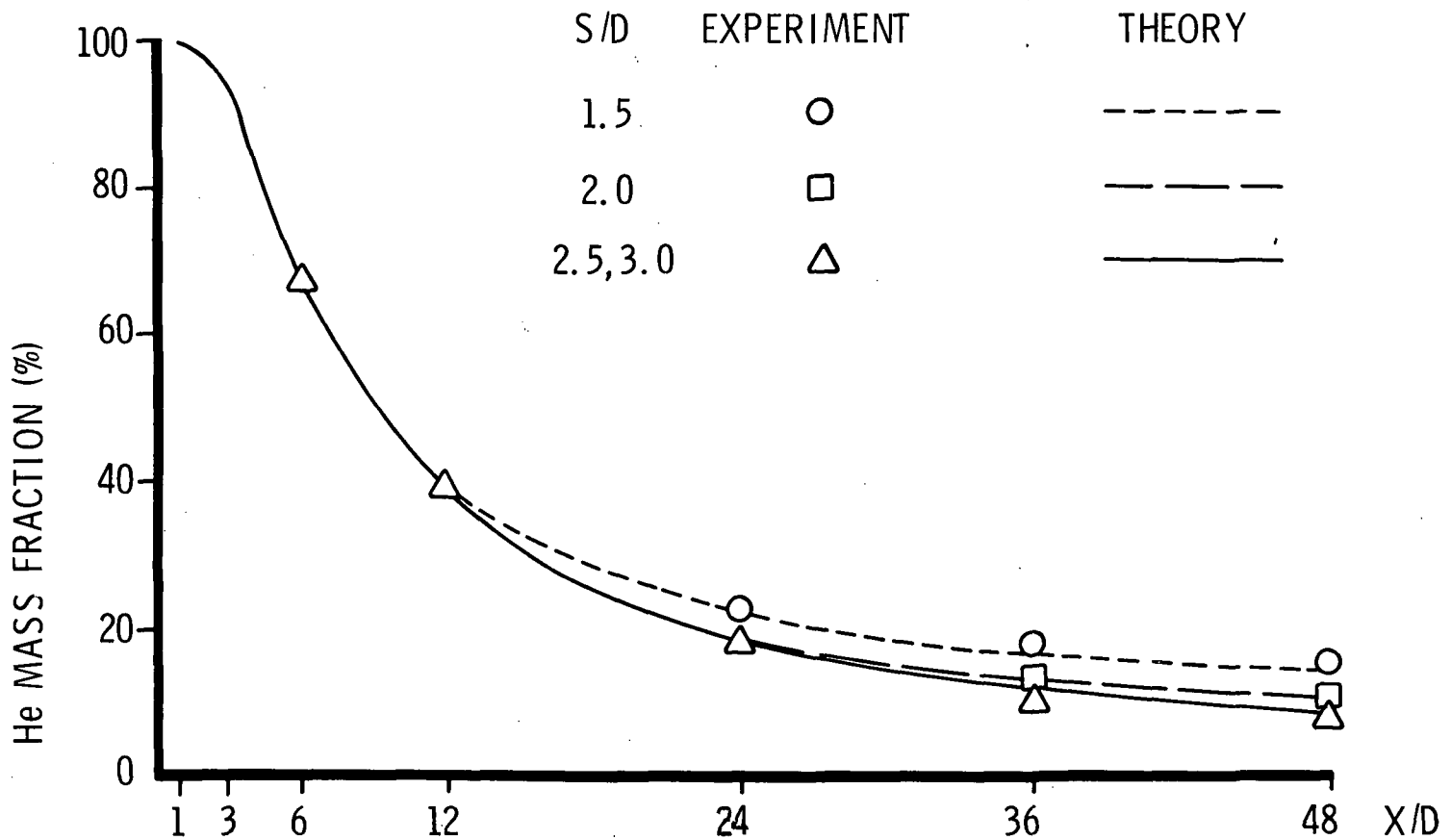

FIG. 26 He CONCENTRATION VS. X/D AT JET CENTERLINE; COMPARISON BETWEEN THEORY AND EXPERIMENT